ELECTRONIC SIMULATION OF

INTESTINAL ACTIVITIES

A NETWORK MODEL OF SMALL INTESTINAL ELECTRICAL ACTIVITIES

by

VICTOR. M. CARBAJAL C., B.Eng.

A Thesis

Submitted to the School of Graduate Studies

in Partial Fulfilment of the Requirements

for the Degree

Master of Engineering

McMaster University

March 1981

Master of Engineering — McMaster University

(Electrical Engineering) — Hamilton, Ontario

TITLE: A Network Model of Small Intestinal Electrical Activities

AUTHOR: Victor M. Carbajal C., B. Eng.

SUPERVISOR: Dr. S. K. Sarna

NUMBER OF PAGES: x, 80

ABSTRACT

An electronic circuit based on a modified version of the four branch Hodgkin-Huxley electrical equivalent circuit (Roy, 1972) has been proposed and implemented to simulate the pattern of the electrical activities present in the muscle cells of the mammalian small intestine.

The analog's implementation comprises two main circuits to simulate these activities. One of them is concerned with generating subthreshold oscillations, while the other is basically a spike-generator circuit. Additional circuitry is included to interface them. Furthermore, the analog provides a parameter set by means of which its performance may be varied. Such settings may alter the intrinsic frequency, the magnitude of the depolarizing phase of the control potential for the response activity to occur, and also the frequency of the electrical response activity.

Four such electronic oscillators, having different intrinsic frequencies, were coupled together in a chain structure with passive elements to simulate "frequency pulling" and "entrainment" . The model qualitatively reproduced the observed pattern of electrical activities in the small intestine.

ACKNOWLEDGEMENTS

I would like to indicate my gratitude to my supervisor, Dr. S. K. Sarna, for the encouragement and expert guidance throughout this project.

I am also very grateful to my wife Lupita,who helped prepare this thesis in its final written version, and for patiently supporting me in the pursuit of my studies.

TABLE OF CONTENTS

LIST OF FIGURES

CHAPTER 1

INTRODUCTION

1.1 General

Smooth muscle cells are small, spindle-shaped with a diameter of usually less than 5 μm and a length of 20-50 μm. The cells are packed closely together to form bundles.

The shape of the cells and absence of alignment of contractile proteins enable smooth muscle to function while undergoing greater changes in length than does skeletal or cardiac muscle. This is necessary for organs such as the bladder or stomach with variable capacities.

Smooth muscle is widespread throughout the body of vertebrates and its contractile activity is vital for normal functioning of the body. The contractile parts of the walls of hollow vessels and cavities such as blood-vessels, the alimentary canal and the urogenital tract are formed from layers of smooth muscle cells which propel, mix and retain the contents. Elsewhere smooth muscle cells are less intimately associated with other tissues and their contraction tends to move one structure relative to another. These include the ciliary muscles and nictitating membrane of the eye, the

pilo-erector muscles of the skin and the anococcygeus and costo-uterine muscles which are attached at one end to bone.

Associated with position and function, smooth muscle cells vary widely in their patterns of activity. For instance, at one extreme, more or less continuous, maintained activity may be required, as in the iris, blood vessels or ureter; whereas at the other extreme, an occasional burst of activity occurs in muscles involved in defecation or pregnancy. Furthermore, tissues such as the urinary bladder or iris contract as a unit, whereas in the ureter or intestine, waves of contraction pass from one end to the other.

The activity of any muscle depends on a number of factors, including the properties of the individual smooth muscle cells, the interaction between cells and the influence of external agents such as nerves, hormones and the physical environment.

The small intestine is a part of the gastrointestinal tract (see fig. 1) and it is represented by a convoluted tube in the abdomen that leads from the stomach to the large intestine. The intestinal wall consists of two concentric smooth muscle layers, sheathed by the mucosa inside and the serosa outside:

1. the outer or longitudinal layer, and
2. the inner or circular layer.

Fig. 2 shows the schematic diagram of a cross section of the gut.

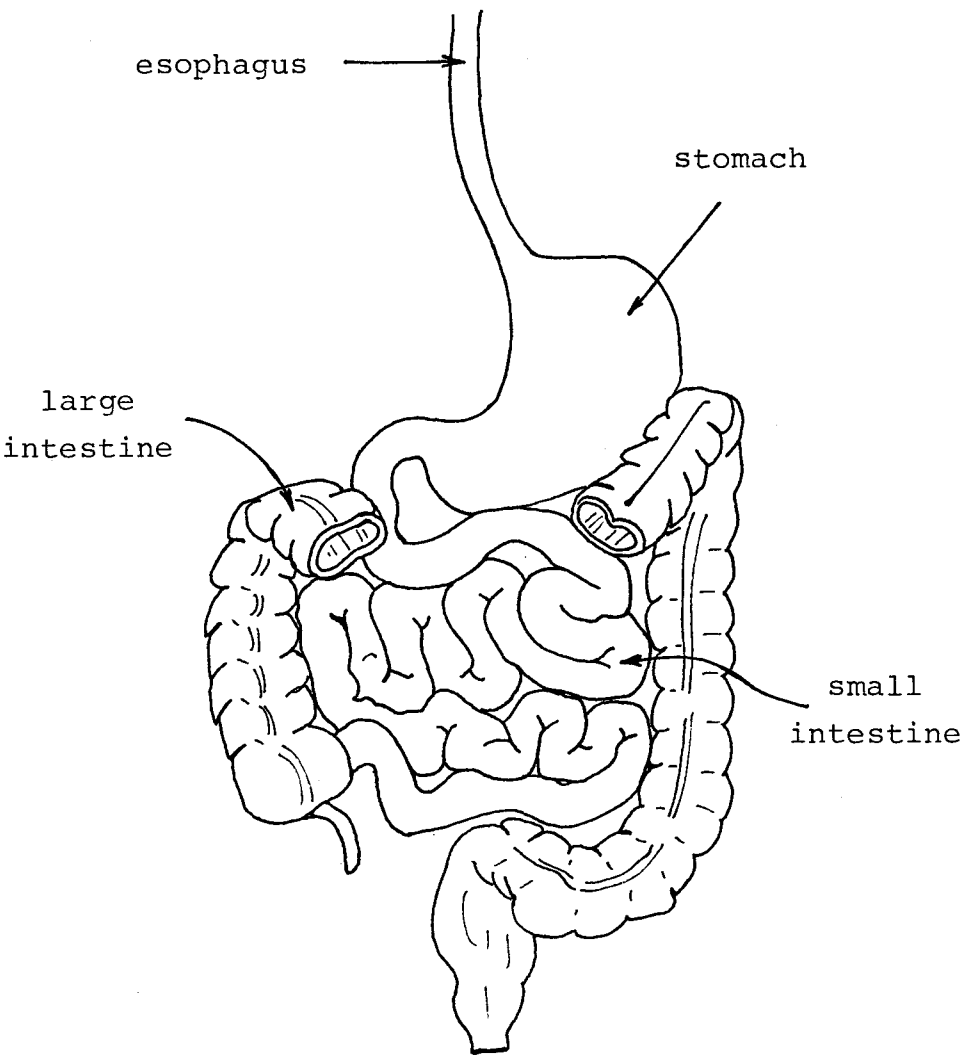

Fig. 1 Shows a simplified diagram of the gastrointestinal tract.

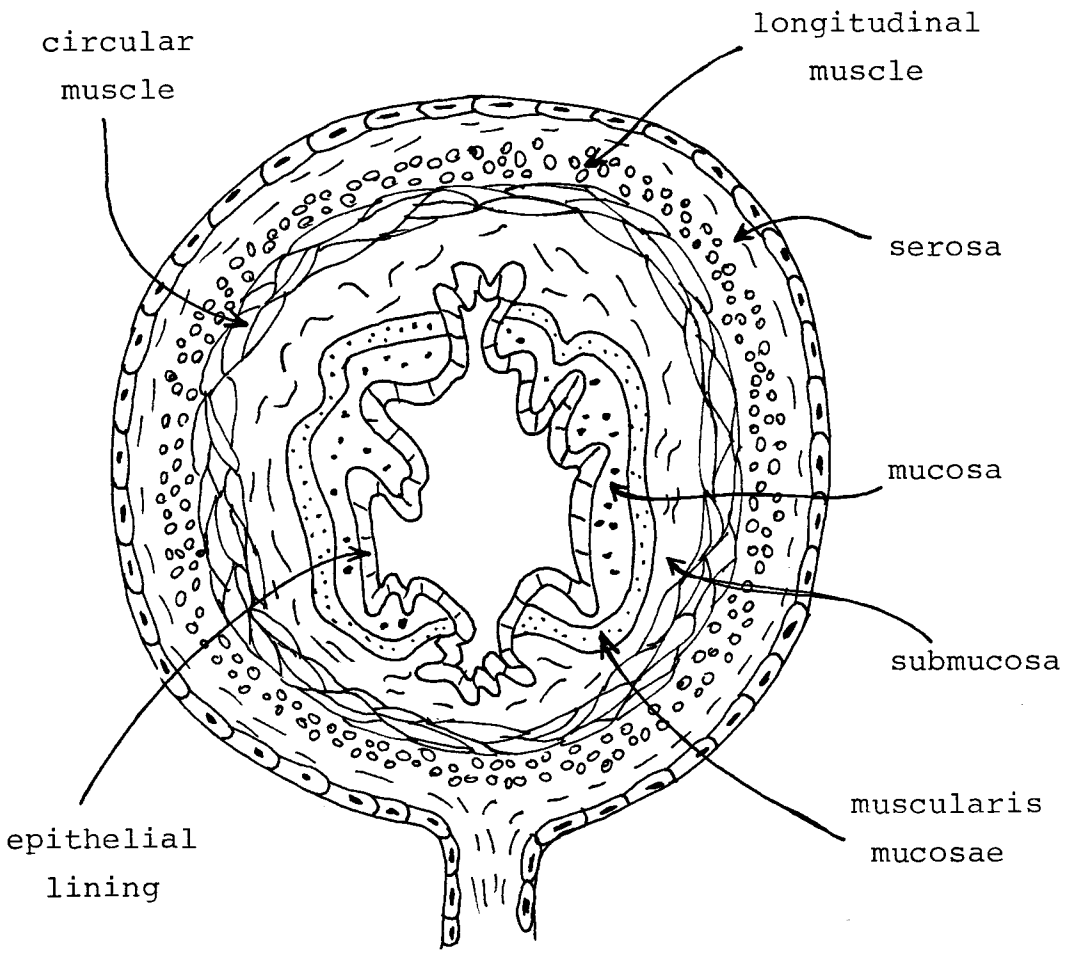

Fig. 2 Typical cross section of the gut.
(Guyton, 1977).

Intestinal motility is regulated through a combination of myogenic, neural and hormonal factors. The muscle contracts to move intestinal contents in two ways: to propel contents toward the caudal end of the tube, and to optimize absorption by bringing the contents into contact with the intestinal wall.

The earliest studies on the electrical activity of the gastrointestinal tract were those of Alvarez and his associates (for a review see Alvarez, 1940). He was able to record the rhythmic electrical activity from the small intestine by using extracellular electrodes connected to an Einthoven string galvanometer with a long time constant. Puestow (1933) who conducted his research using essentially the same techniques confirmed the presence of this activity and reported the presence of an electrical spike activity superimposed on the rhythmic electrical activity. He also suggested that the frequency and duration of the spike activity might be associated with the strength of muscle contractions.

In the late 1930's, Bozler (1938) introduced the use of new amplifiers with an improved frequency-response range into smooth muscle electrophysiology. With this technique, he was able to confirm that electrical activity of the intestinal muscle consisted of spike activity in addition to the rhythmic electrical activity and that the contractile activity was in fact associated with the spikes (Bozler, 1946). After the introduction of intracellular microelectrode recording

techniques to smooth muscle electrophysiology by Bulbring and Hooton (1954), many workers soon applied it to studies of small intestine (Daniel, Honour and Bogoch, 1960; Bortoff, 1961; Kobayashi, Nagai and Prosser, 1966).

The use of this technique clearly showed that the electrical activity of the smooth muscle cells of the gastrointestinal tract has two types of electrical activity (Milton and Smith, 1956; Burnstock, Holman and Prosser, 1963; Daniel and Chapman, 1963; Bass, 1965; Duthie, 1974). One of these activities is called Electrical Control Activity (ECA) and the other Electrical Response Activity (ERA) (Sarna, 1975).

The ECA is rhythmic and omnipresent. Current evidence strongly indicates that control activity is myogenic in nature (Burnstock, Holman and Prosser, 1963). Bortoff (1961) had established that isolated segments of small intestine continue to exhibit control activity in the absence of extrinsic innervation. This control activity was also found to persist after the application of drugs which are known to interfere with transmission of nerve impulses (Holaday, Volk and Mandell, 1958; Daniel, Wachter,Honour and Bogoch, 1960; Daniel and Chapman, 1963). Furthermore, it has been suggested that possibly the origin of this control activity is in the longitudinal muscle layer (Daniel, Honour and Bogoch, 1960) and that it spreads electrotonically to the circular layer (Bortoff, 1961).

The ECA is a regular wave arising from a membrane

potential of -30 to -50 mV (being negative inside membrane) and its amplitude varies from 5-20 mV (El-Sharkawy and Daniel, 1975). The frequency of the ECA depends on the anatomical location from which the recording is made and the species of animal studied (Duthie, 1974). The basic function of the ECA is to control the occurrence in time and space of the electrical response activity. The ERA is of intermittent nature and is associated with muscle contractions (mechanical activity). This activity does not occur by itself, in contrast to the ECA, but only during the maximal depolarized phase of the control potential and assuming that hormonal and neural influences are favourable (Bass, 1965; Daniel, Carlow, Wachter, Sutherland and Bogoch, 1959).

Different aspects of membrane function have been proposed with a view to understanding the maintenance of the membrane potential and the electrical changes connected with the electrical control and response activities (El-Sharkawy and Daniel, 1975). They are based on measurments of extracellular ionic concentrations. So far, none of them has achieved overall acceptance, and the basis of the ionic mechanisms underlaying these electrical activities, ECA and ERA, are still unknown.

1.2 Objectives

The objectives of this thesis are:

a). to implement an electronic oscillator to simulate the small intestinal electrical control and electrical response activities with real life parameters (time and magnitude). Furthermore, the electronic analog must provide a number of variables so that alterations of its basic characteristics may be performed. For instance, parameter changes may be made to modify the intrinsic frequency of the electrical control activity as well as the frequency of the electrical response activity. In addition, response potentials may also be evoked by changing a parameter setting.

b). to bidirectionally couple four such oscillators by using passive elements to simulate observed characteristics of frequency entrainment in the small bowel.

In chapter 2, general information about different types of modelling available to simulate gastrointestinal activities is discussed. Chapter 3 describes the circuits and their characteristics used to implement the electronic analog. Chapter 4 discusses the characteristics of the responses obtained when experimenting with the analog as a single unit. Chapter 5 describes the capabilities of the analog when coupled, and discusses the results obtained when simulating a

chain of four of these analogs coupled together. The conclusions derived from the experimental results and suggestions concerning the applicability of the model to further studies on electronic simulation of electrical activities of the small intestine are proposed in chapter 6.

CHAPTER 2

GASTROINTESTINAL MODELLING

2.1 General

Throughout this thesis the following terminology will be adopted to describe the intestinal electrical activities (Sarna, 1975), and the development and functioning of the electronic analog.

Control potential: denotes one depolarization and repolarization of the membrane potential.

Control wave: denotes the continuing rhythmic electrical control activity recorded at any one site with a monopolar or bipolar recording method.

Intrinsic frequency: denotes the frequency of the control wave at any one site when it is electrically isolated from its neighboring segments.

Electrical control activity (ECA): denotes the totality of the continuing rhythmic electrical activity in any part of the gastrointestinal tract.

Response potentials: denote the rapid oscillations of membrane potential (spikes) in the depolarized state of smooth muscle cells.

Electrical response activity (ERA): denotes the activity in totality of the groups of response potentials in an organ or its parts.

Throughout this thesis, the terms model and analog will be used to mean that which is similar in function but differs in structure and origin from that which is modeled. The making of models is universal in the search for a consistent and instructive picture of nature. An important part of the utility of a model lies in its ability to focus disparate evidence and interpretations into one coherent view. Furthermore, models are valuable only insofar as they raise new questions and suggest new relationships, perhaps leading to new experiments that might not otherwise have been considered. Worthwhile models are predictive, that is, new relevant properties are deducible from them. Unfortunately, the incomplete state of knowledge of the ionic mechanisms that generate different types of electrical activity, the complexity with which the cells are interconnected with neighboring ones, and the controversies over interpretation have so far prevented a complete understanding of the smooth muscle electrical activity, as well as having precluded precision in model-making.

Despite this fact, several models of smooth muscle electrical activity in the digestive tract have been reported during the last twenty years. These models have mainly taken the form of network models, mathematical and computer models,

or electronic models.

2.2 Network models

This group of models was based on the core conductor theory. Several investigators (Abe and Tomita, 1968; Kobayashi, Prosser and Nagai, 1967; Nagai and Prosser, 1963) attempted to use the core conductor properties to explain the spread of smooth muscle electrical activity.

The way in which currents are distributed in a syncytium of coupled cells, that is, what proportion passes on to the other cells, depends on several factors. The most important, however, may be the shape of the syncytium. For instance, if it is a three-dimensional block of cells it will be extremely difficult to make any measurments of membrane properties. On the other hand, if it can be reduced to a long thin thread of only one dimension it will be much easier to work with. One-dimensional structures of this type are known as cables.

Workers in this modelling group assumed a cable structure that consisted of an electrical conductor in the form of a cylinder covered by a sheath of higher resistance and immersed in a conducting medium. They agreed that this was a good description of a single nerve axon in physiological saline, and that it could be applied to a bundle of smooth muscle cells. There are two parameters that describe

the electrical properties of a cable, the space-constant (λ) and the time-constant (τ).

The space-constant is a measure of how far voltage changes spread along the cable. If the voltage in a long cable is changed by an amount V_0 by passing in steady current into the cable at that point, the voltage change V_x at any distance x from that point is given by:

$$V_x = V_0 \exp(-x/\lambda)$$

This means that if λ is large, voltage changes spread for appreciable distances along the cable. High values of membrane resistance or low values of internal resistance lead to large values of λ.

The time-constant is a measure of how rapidly the voltage across the cable membrane changes for a given current; if τ is large the voltages will change more slowly. The time constant is equal to the product of the resistance of unit area of cell membrane, R_m ($\Omega \cdot cm^2$) and the capacitance of unit area of cell membrane, C_m ($F \cdot cm^{-2}$).

The space-constant and the time-constant are all that need to be known to predict the time-course of voltage changes in a cable, but nothing can be said about the absolute size of the changes without an independent estimate of membrane resistance or internal resistance.

Studies from cable-like structures have been used successfully to measure smooth muscle membrane properties and suggested possible mechanisms of spread of electrical activity.

However, some of the major restrictions in extending such studies based on cable theory to smooth muscle may be summarized as follows:

1. the current spread in smooth muscle cells is three-dimensional, so the classical approach of measuring parameters along the axis of current spread is not applicable to smooth muscle cells.
2. many smooth muscle cells are spontaneously active, so the interaction between two active regions has to be considered rather than between an active and a quiescent region as in an axon.
3. since there is no protoplasmic continuity, the path of current spread is not uniform, that is, the current spread over a cell would behave differently than the current spread between cells.

2.3 Mathematical and computer models

Most of the investigation which has been done with mathematical and computer aided modelling is based on the work of Van der Pol (1928). He suggested that many naturally occurring rhythmic oscillations are the result of a relaxation phenomenon. Furthermore, he proposed a differential equation which describes such oscillations, and modified forms of this equation have been widely applied to model the

gastrointestinal electrical activity. For instance the concept of linked relaxation oscillators has been used for several groups to model the small intestinal electrical activities (Nelson and Becker, 1968; Diamant, Rose and Davison, 1970; Brown, Kwong and Duthie, 1971; Sarna, Daniel and Kingma, 1971; Robertson and Linkens, 1974).

Nelson and Becker (1968) were the first to propose that the intestinal electrical activities could be simulated using a chain of relaxation oscillators. They used two forward-coupled Van der Pol oscillators and demonstrated the effect of frequency entrainment or pulling (depending on the degree of coupling factor) of the distal oscillator (having the lower intrinsic frequency) by the proximal one (having the higher intrinsic frequency).

It has been demonstrated that if the small intestine is divided into small segments, each segment will have a frequency of its own, called intrinsic frequency. The gradient of intrinsic frequency in the small intestine reduces distally, therefore each segment of the small intestine may be seen as an independent oscillator. However, when the small intestine is intact; that is, the oscillators are coupled, the proximal higher frequency oscillators will tend to pull the frequency of distal lower frequency oscillators to that of their own. Accordingly, frequency pulling is a fundamental characteristic of relaxation oscillators, and will depend upon the amount of coupling and the intrinsic frequency dif-

ference between oscillators.

The relaxation oscillator model was further refined by Sarna, Daniel and Kingma (1971) to simulate the experimentally observed characteristics of electrical control activity in dog small intestine. They presented an analog computer simulation of the electrical control activity in dog small intestine using sixteen bidirectionally coupled generalized Bonhoeffer-Van der Pol oscillators.

More recently, modelling has been attempted using an autorhythmic form of the well known Hodgkin-Huxley (1952.d) equations as a unit oscillator. Linkens and Datardina (1977) in a digital simulation study have shown that coupled Hodgkin-Huxley oscillator chains could produce similar behavior to the coupled Van der Pol oscillator model even for large wave form asymmetry. It was also shown (Patton and Linkens, 1977) that these units, when intercoupled, reproduce most of the solutions obtained from coupled Van der Pol oscillators.

Unfortunately, due to the complexity of the equations, digital simulation of chains of these units has become quite difficult and time consuming, even for a few oscillators and a small number of oscillation periods. An alternative to this approach is to construct electronic analogs of the squid axon membrane, based on the original voltage-clamp observations of Hodgkin-Huxley (1952.a,b,c). The use of the more direct hardware for modelling has much to recommend it. In the

first place, it is simpler, as the nonlinear equations are complicated to program. Adjustments of the various parameters is very convenient, involving simply changing a potentiometer setting or a capacitive value. In addition, considerable insight into membrane behavior can be realized, since the response of the analog to parameter changes is simultaneously observable on an oscilloscope.

2.4 Electronic models

Most of the work done in electronic modelling has been somewhat related or based on the four branch Hodgkin-Huxley electrical equivalent circuit for the squid axon membrane. It has sometimes been used in a modified form to describe the behavior of biological membrane other than the squid axon membrane, and it seems that they will be discarded only when the molecular basis of membrane activity may finally be unravelled.

Figure 3 shows the Hodgkin-Huxley membrane electrical equivalent circuit for the squid axon membrane. The first branch represents the membrane capacitance C_m, which was assumed constant. The remaining three branches provide the current pathways for each of the three separate components of the ionic current across the membrane. These components are the sodium ionic current, the potassium ionic current and the leakage current, the term leakage being used for the

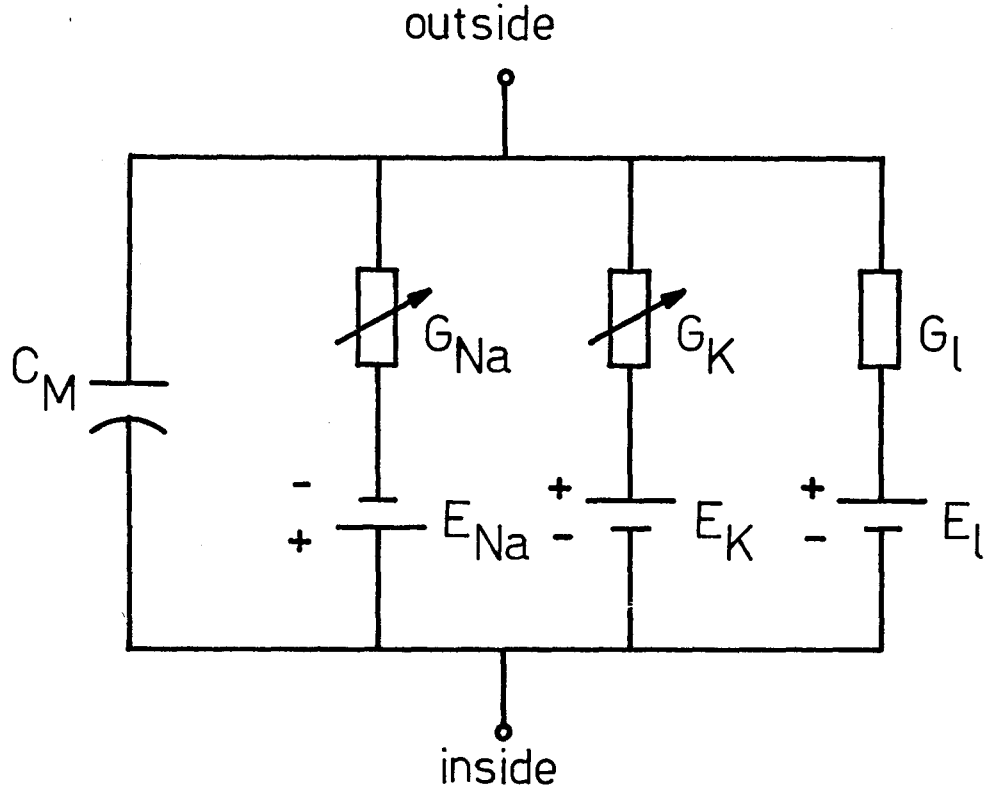

Fig. 3 The Hodgkin-Huxley electrical equivalent circuit for the squid axon membrane. C_m: membrane capacitance. G_{Na}, G_K and G_l, are the electrical conductances of the membrane to sodium, potassium and leakage ions, respectively.

lumped current contribution of all ions other than sodium and potassium. The conductance of the membrane to each of these three types of ions is depicted in fig. 3 as the electrical conductances G_{Na}, G_K and G_l, respectively. Each of these conductances is placed in series with an electromotive source whose magnitude equals the Nernst equilibrium potential for the respective ion.

The early work of Lewis (1968) using this approach showed that such circuits are capable of reproducing many of the well known nerve and muscle action potential wave shapes, but they are unsuitable for reproducing chains of such oscillators because of the large number of components used.

Lewis' model, while simulating membrane phenomena closely, was relatively complex. Its complexity was in part due to the fact that it did not simulate the variable sodium and potassium conductances of the Hodgkin-Huxley model directly. Instead, electronic multipliers were used.

Roy (1972) following a suggestion by Lewis, built a simple analog for the squid axon membrane that used the variable drain-to-source conductance G_{DS} of junction field-effect transistors (FET's) to simulate the sodium and potassium ionic conductances. Furthermore, operational amplifiers and shaping networks were used to give the correct time and voltage dependency to the conductance paths.

This electronic model was further refined by Gulrajani and Roberge (1976), who added further components

to accurately simulate the transients in sodium and potassium conductances of the Hodgkin-Huxley dynamics. Their analog was used to investigate the mechanisms of spontaneous activity in a patch of biological membrane. Furthermore, they showed that with appropriate modifications the analog could generate subthreshold oscillations.

They also demonstrated that incorporation of additional conductance branches (G'_{Na}, G'_{K}) to the basic Hodgkin-Huxley circuit gave bursting spikes on top of the slow subthreshold oscillations seen in cell R_{15} of the Aplysia abdominal ganglion (Gulrajani, Roberge and Mathieu, 1977).

Intestinal electronic modelling was first initiated by the work of Brown, Duthie, Horn and Smallwood (1975). They developed an electronic circuit having a feedback arrangement comprising two operational amplifiers and several resistors to produce an alternate charge and discharge of a capacitor placed between them. Their model was run about 600 times faster than real time, and its magnitude was considered as a logical output for display purposes of its phase relationship when coupled. That is, the relative phase shifts of coupled oscillators at any time was made available by scanning their outputs and giving an output of '1' if the oscillator output was positive, and '0' if it was negative.

Patton and Linkens (1978) showed that an electronic model comprising a number of coupled Hodgkin-Huxley type nonlinear oscillators is capable of reproducing physiologi-

cal phenomena observed in electrical recordings from the mammalian digestive tract, and also demonstrated the advantages of this model over simpler Van der Pol oscillators. Very recently, this circuit was slightly modified by Linkens (1980) to simulate the simultaneous occurrence of both the electrical activities in the small intestine. He showed that a Hodgkin-Huxley type oscillator is capable of two modes of oscillation equivalent to control waves and response activities. Furthermore, he demonstrated the effect of frequency entrainment when the models were forward-coupled together.

Apart from the initial modelling work of Nelson and Becker (1968), Linkens' model shows the response potential effects which have been largely ignored in most of gastrointestinal modelling studies. Furthermore, this model was the first described in physiologically meaningful ionic terms as far as smooth muscle cell modelling is concerned. Since precise matching of the Hodgkin-Huxley dynamics is not yet possible in intestinal modelling, Linkens' model is based on a simple approach which does retain the basic characteristics of the Hodgkin-Huxley original circuit. It comprises a membrane capacitance C_m plus two parallel ionic conductance paths each represented by a field- effect transistor (FET) to simulate the sodium and potassium dynamics. However, the model suffers from a lack of precise and independent parameter setting adjustments to achieve either or both the modes of rhythmic oscillations, as well as of a

real magnitude and frequency output.

CHAPTER 3

IMPLEMENTATION OF AN ELECTRONIC OSCILLATOR TO SIMULATE THE ELECTRICAL ACTIVITIES OF THE SMALL INTESTINE

3.1 Development of the electronic analog

Initially an attempt was made to use the approach of Gulrajani and Roberge (1976) to simulate the electrical control and electrical response activities, but it was found to be extremely hard to assume representative parameters for the smooth muscle cells. Such parameters, for the model to work efficiently, must necessarily involve a correct knowledge of the variations of the conductances of sodium and potassium with depolarization, as well as the magnitudes of the rise times, fall times, inactivation times and recovery from inactivation times of the conductance transients. Otherwise, it was not worth using such a sophisticated model. Thus, needless to say that since precise values of such parameters in smooth muscle cells are not currently available, the proposed electronic analog in this thesis has been based on a modified version of the membrane electronic analog due to Roy (1972) together with extra circuitry to fully simulate the electrical control and electrical response activities.

A block diagram of the complete electronic analog is shown in fig. 4. Clearly, it is seen that the proposed electronic analog comprises three main circuits represented by blocks B1, B2, and B3, plus an output circuit represented by block B4.

The first circuit denoted by block B1 generates the slow oscillations to simulate the electrical control activity, ECA. Block B2 represents a spike generator circuit used to reproduce the electrical response activity, ERA. Finally, block B3 consists of an interfacing circuit which will be used to decide whether or not the activation of the ERA circuit will occur. Its functioning is only partly dependent on the ECA circuit, since the activation of the ERA circuit is also dependent on extrinsic factors as will be shown later.

The adder stage represented by block B4 was included in order to provide the output of the electronic analog. Thus, the simulated small intestinal electrical activities will be always monitored after this stage.

The following sections of this chapter will deal with a detailed explanation of the functioning of each of the above mentioned circuits represented in the block diagram of fig. 4. It should be noted that no intrinsic similarity between the electronic analog circuit and biological process in the membrane smooth muscle cell was attempted, but rather the proposed analog circuit was used to reproduce qualitatively as closely as possible the electrical activity observed

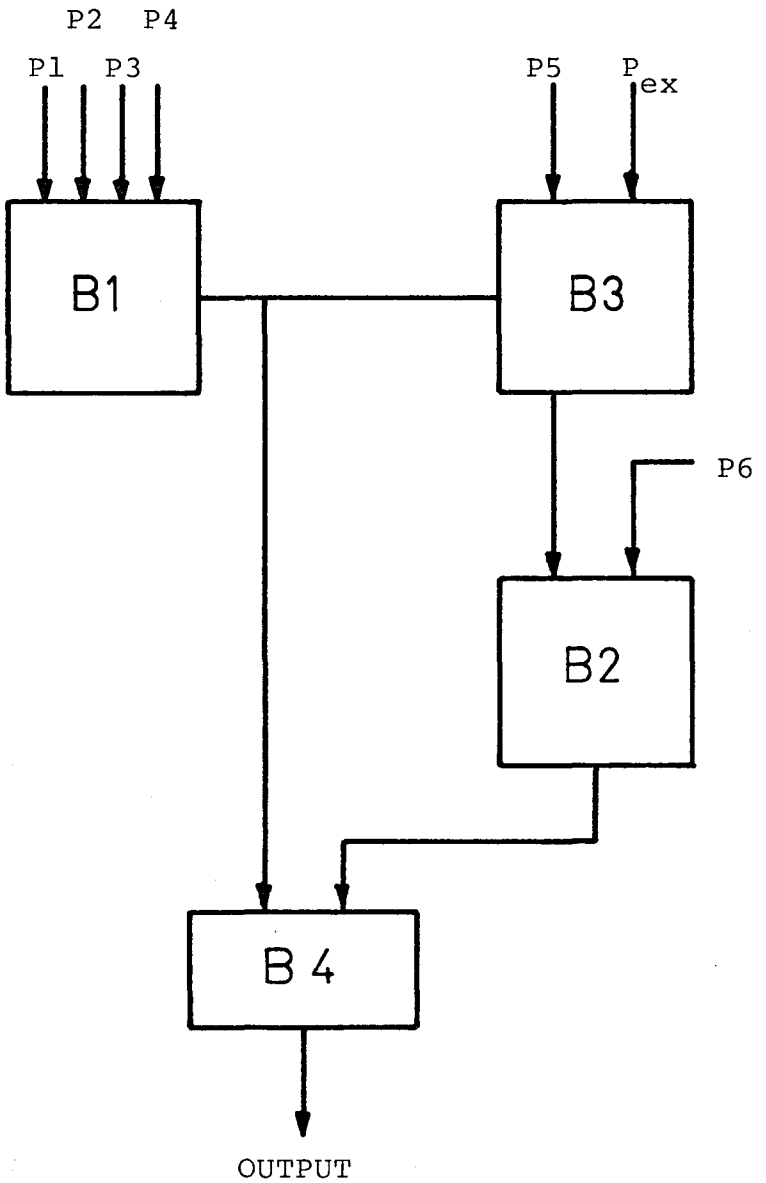

Fig. 4 Block diagram of the electronic analog used to simulate the electrical control and electrical response activities. B1: represents the ECA circuit. B2: represents the ERA circuit. B3: represents the interfacing circuit. B4: represents an adder stage which provides the output of the electronic analog. Potentiometers are denoted by P's.

from intestinal recordings.

3.2 The ECA circuit

The implementation of this circuit is to provide the slow oscillations observed in experimental electrical recordings from the smooth muscle cells of the small intestine. Fig. 5 shows the electrical diagram corresponding to the ECA circuit, and it can be noted that two field-effect transistors (FET) were used to simulate the variable sodium and potassium conductances.

The changes in these conductances may be easily achieved with a FET due to its electrical structure. That is, under conditions of low applied drain-source voltage (-200 mV $< V_{DS} <$ $+200$ mV) its current/voltage characteristic I_{Drain} against V_{DS}, is almost linear. Furthermore, the drain-source conductance G_{DS}, is controlled by the voltage between the source and gate terminals.

Therefore, two conductance channels in parallel with a capacitance C_m, form the complete oscillator unit for the ECA circuit to be simulated. The sodium and potassium conductances are each represented by a 2N4340 N-channel field-effect transistor (FET) in series with a resistor, and an equilibrium potential of approximately +100 mV and -80mV, respectively. The third leakage ionic channel present in Roy's circuit, which is a lumped contribution of all ions

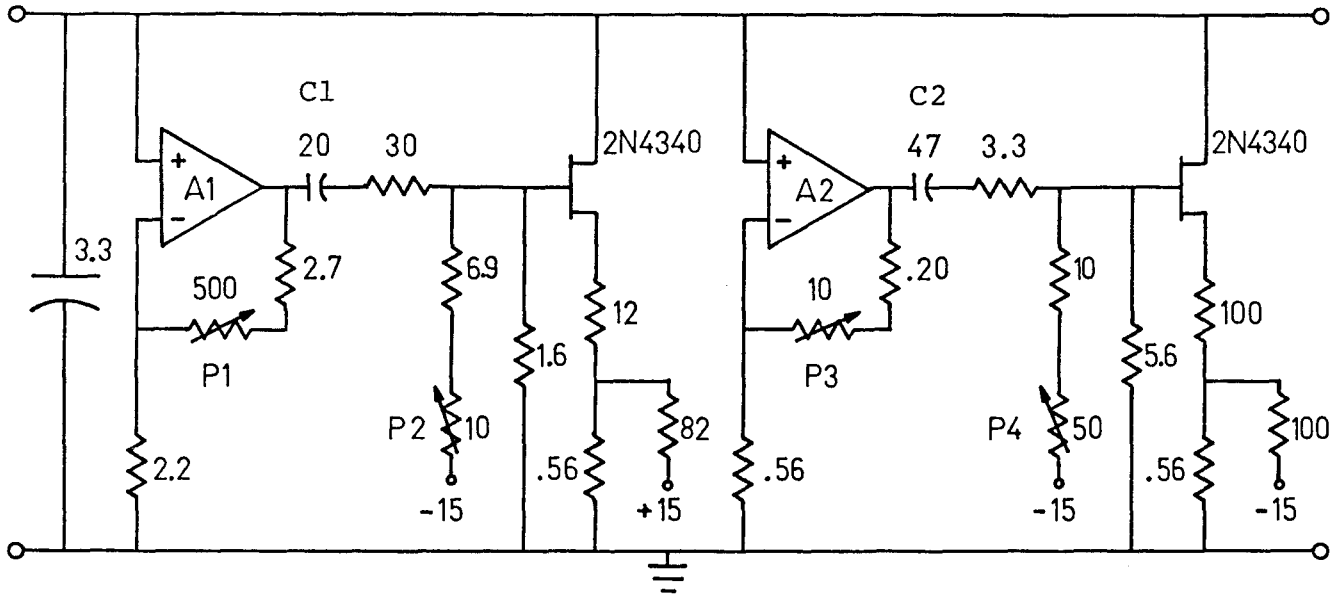

Fig. 5 Electrical circuit to simulate the Electrical Control Activity, ECA. Amplifiers A1 and A2 are of type μA741. All component values are in KΩ and μF unless otherwise indicated.

other than sodium and potassium, has been excluded in order to simplify the circuit, since experimental results have not shown precisely the role of this ionic channel in the intestinal control potential.

The rationale behind using a field-effect transistor to model G_{Na} or G_K is based on the future possibility of matching the FET-conductance curves against depolarization curves of the smooth muscle membrane dynamics, by making changes in V_G proportional to the depolarization. This can be achieved by interposing a more elaborate wave-shaping network between the V_{DS} and V_G of the FET, such that for a change in V_{DS}, the waveform at the gate will result in the total conductance G_{DS} exhibiting the correct smooth muscle membrane conductance.

Since precise data concerning the ionic mechanisms of the membrane in the smooth muscle cells are still unknown, a simple additional circuitry is included to make the conductances both time and voltage dependent.

The sodium and potassium conductances channels are each controlled by a variable-gain operational amplifier (from fig. 5, A1 and A2) in the noninverting mode together with a waveshape network designed to provide the required inactivation time. These amplifiers were also introduced to isolate the FET's from the circuit determining the time dependence of the conductances, and to increase the low drain-source voltage to a larger value in order to obtain

the required change in such conductances. Therefore, voltage dependency of the conductances is given by the amplified feedback of the drain-source voltage, via operational amplifiers A1 and A2.

The waveshape network introduced in the feedback path, in both the channels, consists of an RC circuit. It serves to modify the value of the conductances for a given voltage between drain and source. Therefore, the conductances will become time-dependent.

The value of the capacitor C_m was 3.3 μF, and the intrinsic frequency was selected by changing the gain (P1,P3) and bias (P2,P4) potentiometer settings. For larger frequency variations, another value of C_m may be selected, since the waveshape output is not very much affected.

It should also be noted that a necessary condition for oscillations to occur in this circuit is that the sodium and potassium currents are never equal and opposite; that is, the potassium fall time should exceed the sodium recovery from inactivation time. As the sodium and potassium feedback coupling capacitors are quite different, 20 μF and 47 μF, respectively, it is not difficult to arrange for the above condition to be satisfied.

Summarizing, the ECA circuit has four parameter settings, denoted by potentiometers P1 to P4 in fig. 5, which allow the user to select the intrinsic frequency and shape of the oscillations.

3.3 The interfacing circuit

This stage has been introduced in the analog as an interface between the ECA and the ERA circuits. In this way, the electrical control activity controls the electrical response activity, and hence the contractions (mechanical activity).

Although there is strong evidence indicating that the electrical response activity is associated with mechanical response of the gastrointestinal tract, it is not known altogether the mechanisms for triggering this contractile activity. Furthermore, it has been demonstrated (Bortoff, 1976) that both the rhythmicity and the polarity of intestinal contractions can be ascribed to properties of the electrical control activity.

Rhythmicity is related to the fact that control potential depolarizations periodically increase the excitability, or probability of response potentials. Since excitability is also influenced by neural and hormonal factors, the number of response potentials and the resulting contraction associated with the control potential of course are governed by the interplay of all three factors, but the electrical control activity sets the basic pattern of the mechanical event. For example, Daniel and Chapman (1963) cited that the electrical response activity occurs in response to the occurrence of a control potential and in re-

sponse to the release of acetylcholine (ACh) by the vagal fibers.

It is now well known that the main electrical wave, the ECA, is present all the time in most of the gastrointestinal tract even when the muscle is not contracting. This activity is represented by spontaneous oscillations arising from a resting membrane potential of about -30mV. In addition, it has been demonstrated that when ACh is present around the smooth muscle cell membrane the control potential exhibits a further depolarization. This situation will cause the threshold level to be reached by the control potential, and hence electrical response activity will be present. This activity will last as long as the depolarized phase of the control potential remains above that threshold level, and consists of several response potentials (spike-like) superimposed on top of the control potential. The magnitude of the contractile response is related to the number of spikes occurring during this period. Repolarization of the control potential normally terminates any existing spike activity, resulting in muscle relaxation.

The idea behind using this interfacing circuit between the ECA and the ERA circuits, is to decide whether or not the effect of a given extrinsic factor (e.g. ACh) has been enough for the depolarized phase of the control potential to reach the threshold level. If it is so, the ERA circuit will be activated and response potentials will appear

on top of the control potential. Otherwise, the control potential will remain subthreshold and no mechanical activity will occur.

Fig. 6 shows the diagram of the electrical circuit corresponding to this stage. The initial buffer amplifier A3 (μA741) is connected to provide a variable gain to simulate the effect that ACh may have over the control potential. This effect may further be varied by adjusting the potentiometer setting P_{ex}.

Operational amplifier A4 (μA741) is connected as a comparator in a noninverting configuration. It compares the magnitude of the control potential, as a result of the variation in P_{ex} (ACh effect), with a selected threshold voltage V_{TH}, which can be further varied by changing the potentiometer setting P5.

Fig. 7.a shows the configuration for A4 acting as a latching comparator or level detector with hysteresis. It is one of the most versatile and useful of the comparator circuits, and can be designed to change output states whenever the input passes through any selected reference voltage V_{TH}. The absolute voltages of the two output states are selected by using appropriate zener diodes. In this case, since only positive values of the output will be required, a 1N758A zener diode is used.

The functioning of the latching comparator will determine whether or not the control potential has reached the

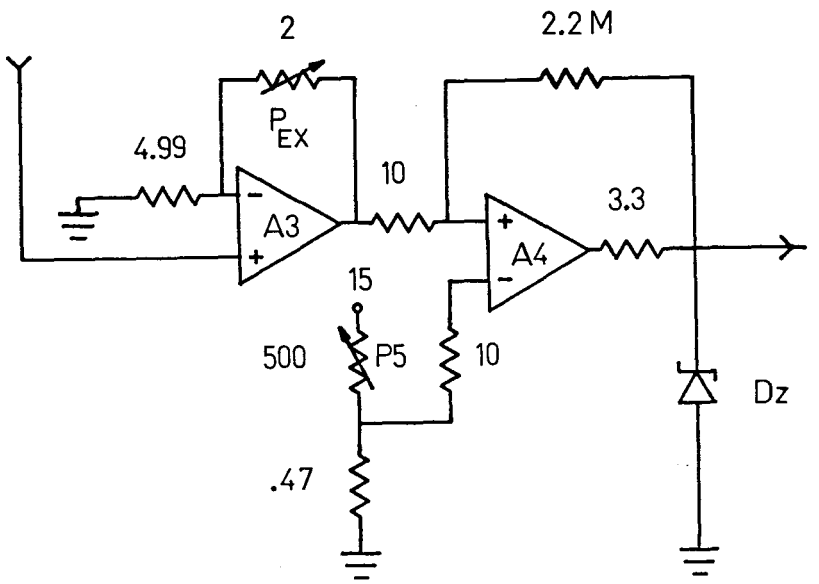

Fig. 6 Electrical diagram of the interfacing circuit used between the ECA and the ERA circuits. Amplifiers A3 and A4 are of type μA741. Diode zener is type 1N758A. All component values are in KΩ unless otherwise indicated.

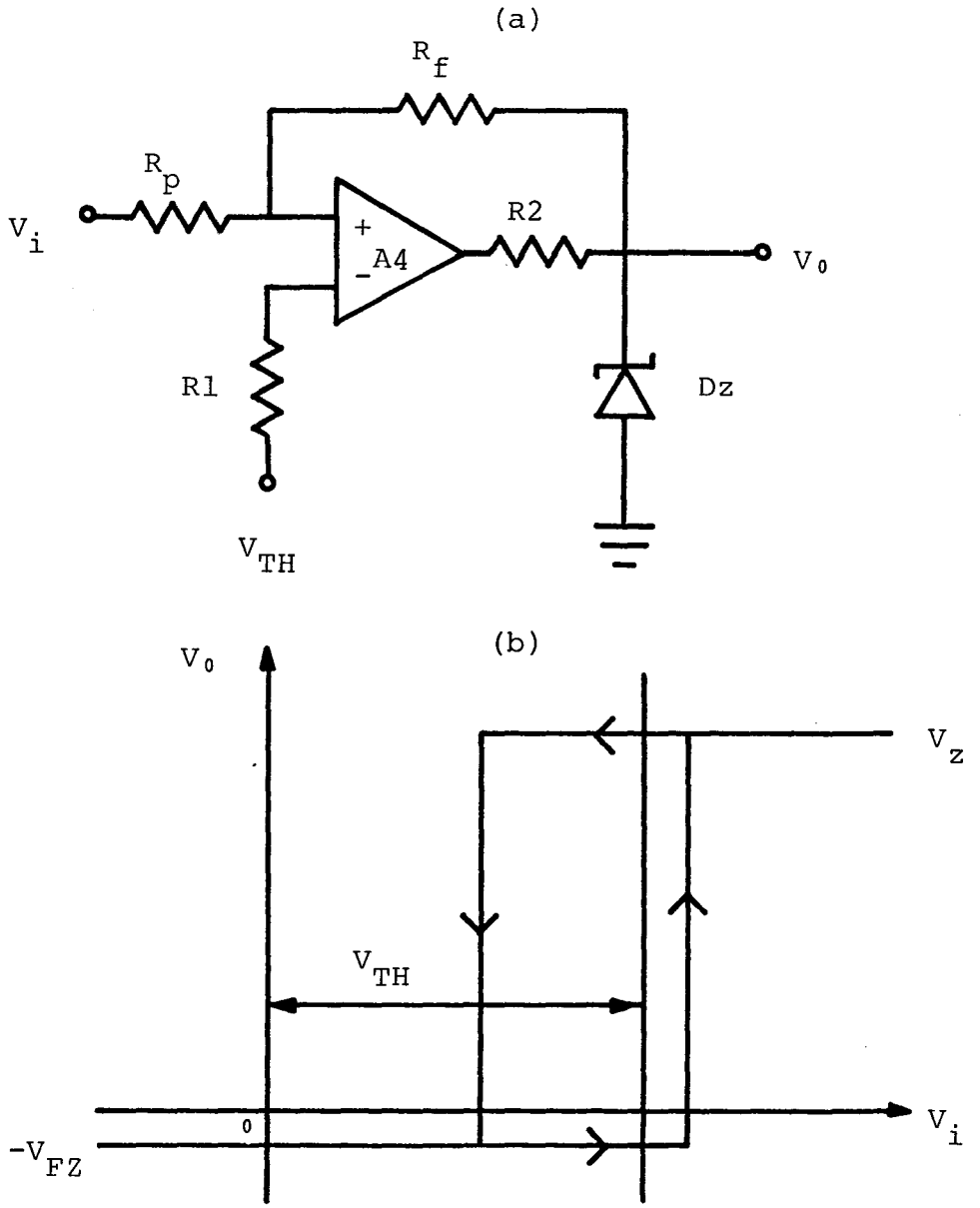

Fig. 7 Noninverting level detector with hysteresis (a), and its transfer function (b). R2: resistor which establishes correct current in Dz. R_f:feedback resistor which establishes hysteresis. R_p: part of hysteresis feedback circuit. V_{TH}: reference voltage used to establish trip voltages. V_z: breakdown voltage of Dz. V_{FZ}: forward breakdown voltage of Dz.

reference voltage V_{TH}. In response to this determination the output voltage will assume one of the two possible states. Referring to fig. 7.b, the output voltage states are:

$$+V_Z \quad \text{if} \quad V_i > \{(V_{TH}(R_p + R_f) - V_{FZ} \cdot R_p)/R_f\}$$

$$-V_{FZ} \quad \text{if} \quad V_i < \{(V_{TH}(R_p + R_f) - V_Z \cdot R_p)/R_f\}$$

According to the above expressions, if the output from the latching comparator A4 is $+V_Z$, that will mean that the control potential has become greater than the threshold value V_{TH}. On the other hand, the output of this comparator will always be $-V_{FZ}$ whenever the control potential is below V_{TH}, and hence in this case no electrical response activity will occur. However, for the former case and due to its condition, response potentials will appear on top of the control potential and they will last as long as $V_i > V_{TH}$.

3.4 The ERA circuit

The implementation of this circuit is to provide the observed response potentials when mechanical activity is present in smooth muscle cells. Fig. 8 shows the electrical diagram of the proposed ERA circuit which generates the response potentials. It consists of a timer IC1 (NE555) together with 9 bipolar-junction transistors (BJT's). NPN transistors are SK3011 or similar types, while PNP transistors are

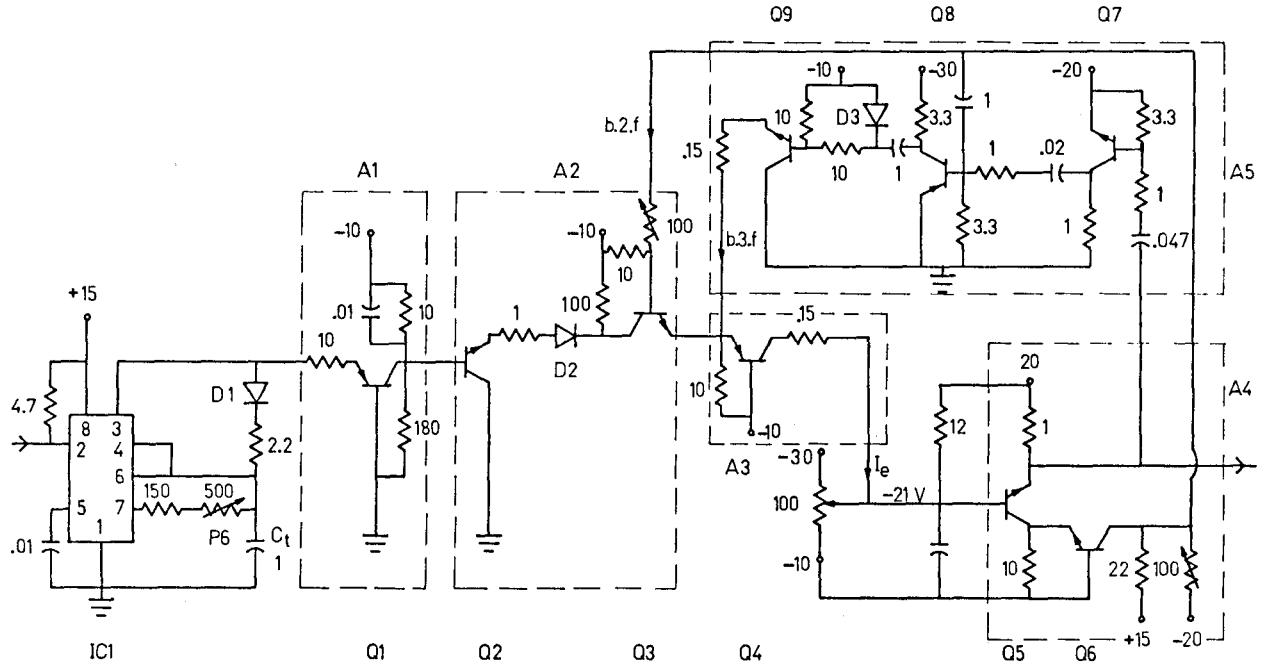

Fig. 8 Electrical circuit to simulate the electrical response activity, ERA. Timer IC1 is of type NE555. NPN transistors: SK3011 or similar types. PNP transistors: SK3004 or similar types. Diodes: 1N4454 or similar types. All component values are in KΩ and μF unless otherwise indicated.

SK3004 or similar types.

The first part of the ERA circuit consists of a timer IC1 to generate pulses of variable frequency, ranging from 2 to 15 Hz, by adjusting the potentiometer setting denoted by P6 in fig. 8. Then, the remaining part of the circuit will further process these pulses to generate the spike-like wave shape characteristic of the response potentials.

The electrical circuit for the timer IC1 is shown in fig. 9, it is a simplified astable circuit configured for positive pulses and gated by the output of the latching comparator A4 as shown in fig. 6. The values of resistor R1 and potentiometer P6, govern the output high time, t_1, and the output low time, t_2, respectively. In this case, the value of potentiometer P6 is made much greater than the value of resistor R1, so that the portion of the total timing interval governed by P6 will be dominant. Under these conditions, t_2 approximates T, so it may be said that $T \simeq 0.693 \cdot P6 \cdot C_t$.

Furthermore, because the timing period t_1 is a very small fraction of T, errors in its value will be reflected as a very small percentage of the total period T. Therefore, the inaccuracy and temperature instability introduced by diode D1 in charging C_t can be neglected for this case, as they are scaled down by the ratio of t_1 to T.

The timer is gated by holding pin 4 (reset) low. This holds the output low, which in turn causes C_t to discharge all the way to zero while the circuit is disabled. Normally

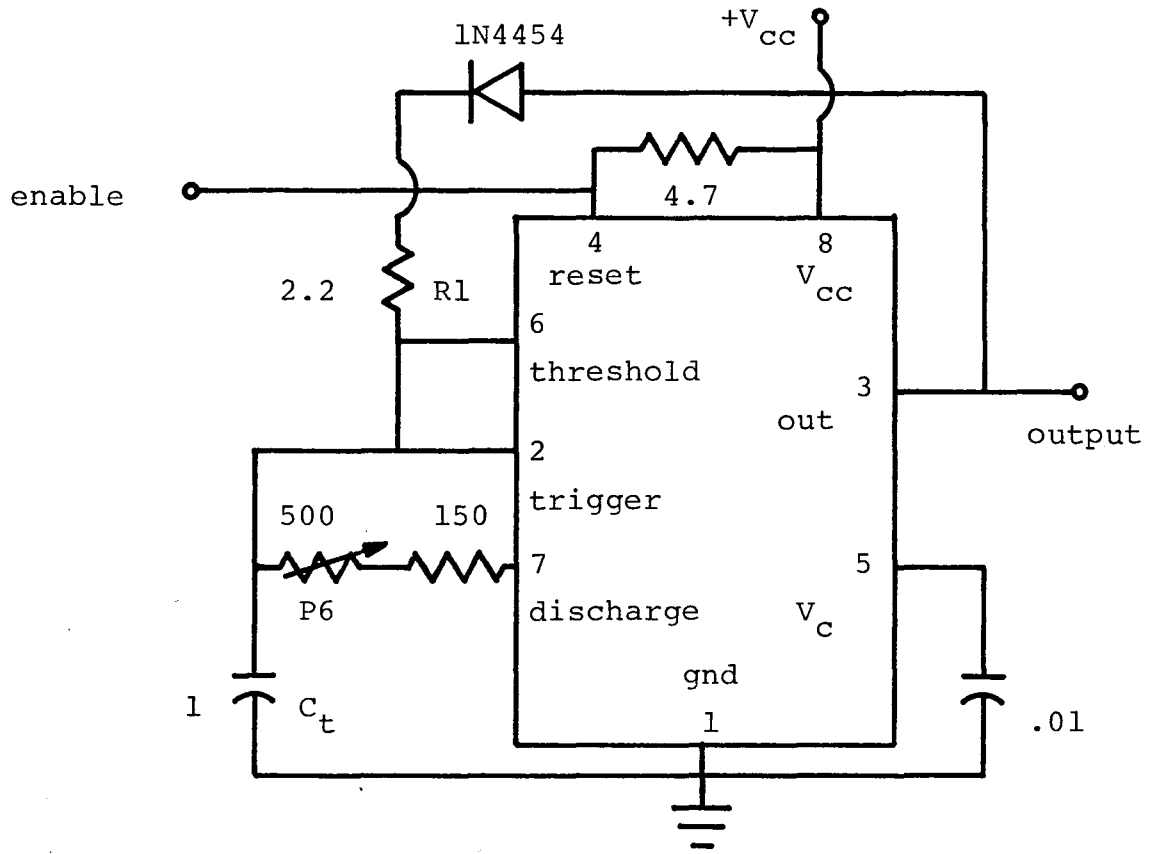

Gated timing:

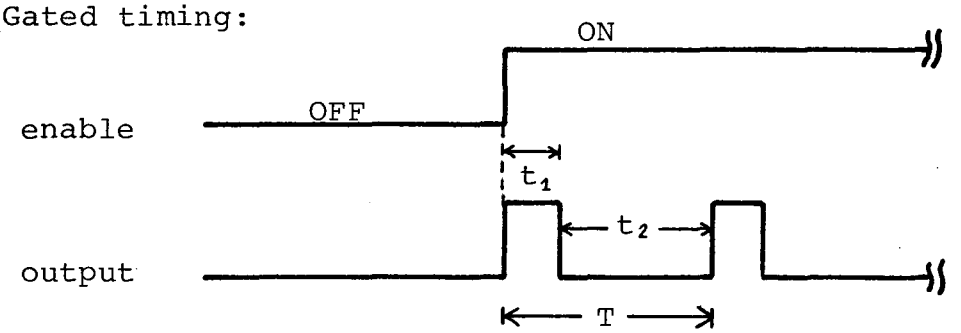

Fig. 9 Gated simplified 555 astable circuit. if R1 << P6, $t_1 << t_2$, and $t_2 \simeq T$ then $T = 0.693 \cdot P6 \cdot C_t$. All component values are in KΩ and μF unless otherwise indicated.

this would cause a first cycle error as C_t charges from zero up to $2(V_{cc})/3$ and then subsequently charges from $V_{cc}/3$ to $2(V_{cc})/3$. However, since t_1 is such a small fraction of the total period, T, this error has a correspondingly small effect on the total period. The circuit may be said to be semi-synchronous, since it starts up immediately with a positive-going output pulse but does have a very slight error in period T of the first cycle compared with subsequent cycles.

The train of positive pulses coming out of the timer IC1 will be used to generate the response potentials through the remaining second part of the ERA circuit as shown in fig. 8. It can also be seen that when timer IC1 is disabled there will be no pulses coming into the remaining circuit, and hence no response potentials will occur. But as soon as timer IC1 is enabled, this remaining circuit will in turn be activated and produce response potentials.

The ERA circuit as shown in fig. 8, will deliver spikes of approximately 10 volts in magnitude, but they are further processed and scaled down for their correct representation at the analog's output. Their waveshape, however, resembles that of response potentials seen in smooth muscle cell electrical recordings when mechanical activity is present.

In addition to the timer IC1, the remaining ERA circuit consists of one three-stage input amplifier represented by blocks A1, A2, and A3, in dotted frames of fig. 8. This

amplifier stage feeds current I_e into an RC circuit, and into a feedback path which also has an amplifier stage.

Under zero or low magnitude pulse stimulation, transistor Q5 is in cut-off state, then feedback path b.3.f may be neglected and no response potentials will be generated. On the other hand, when the magnitude of pulse stimulation is large enough for transistor Q5 to get out of cut-off, block A5 begins to have an effect which will eventually produce response potentials. This block A5 is mainly used to shape the response potentials by producing momentary increases of current, I_e, causing the desired waveshape. This feedback path has a nonlinear transfer function similar to that of differentiating pulse shapers, and was chosen as a compromise between what can easily be realized with electronic components and what corresponds to the desired shape of the response potentials. Furthermore, the shape of these response potentials can be varied over a wide range by alterations to block A5.

Summarizing, the ERA circuit is set to generate response potentials when stimulated; otherwise, it remains quiescent. There is only one explicit variable parameter to adjust in order to modify its output, and that corresponds to frequency variations made with potentiometer P6 shown in fig. 8. Further alterations of the waveshape of response potentials can be done by changing the value of some components in block A5.

CHAPTER 4

THE ELECTRONIC OSCILLATOR AS A SINGLE UNIT

4.1 The complete electronic analog

A diagram of the complete electrical circuit of the proposed analog to simulate the small intestinal electrical activities is shown in fig. 10. It is the result of the combination of the circuits described in previous chapters, plus the introduction of an adder and an inverting stage represented by operational amplifiers A5 and A6, respectively.

Amplifier A5 (μA741) was connected as a summing inverter configuration. Its output is the inverted algebraic sum of the input signal voltages coming from the ECA and ERA circuits, appropriately scaled by the resistance R_{f_5}. Since the characteristic of this configuration is the fact that linear signal mixing takes place at the summing point without interaction between inputs, its output will indeed represent the analog's output. Thus, electrical control and electrical response activities will be always monitored from this point, denoted by M in fig. 10.

Amplifier A6 (μA741) was connected in an inverting configuration in order to invert the signal coming from

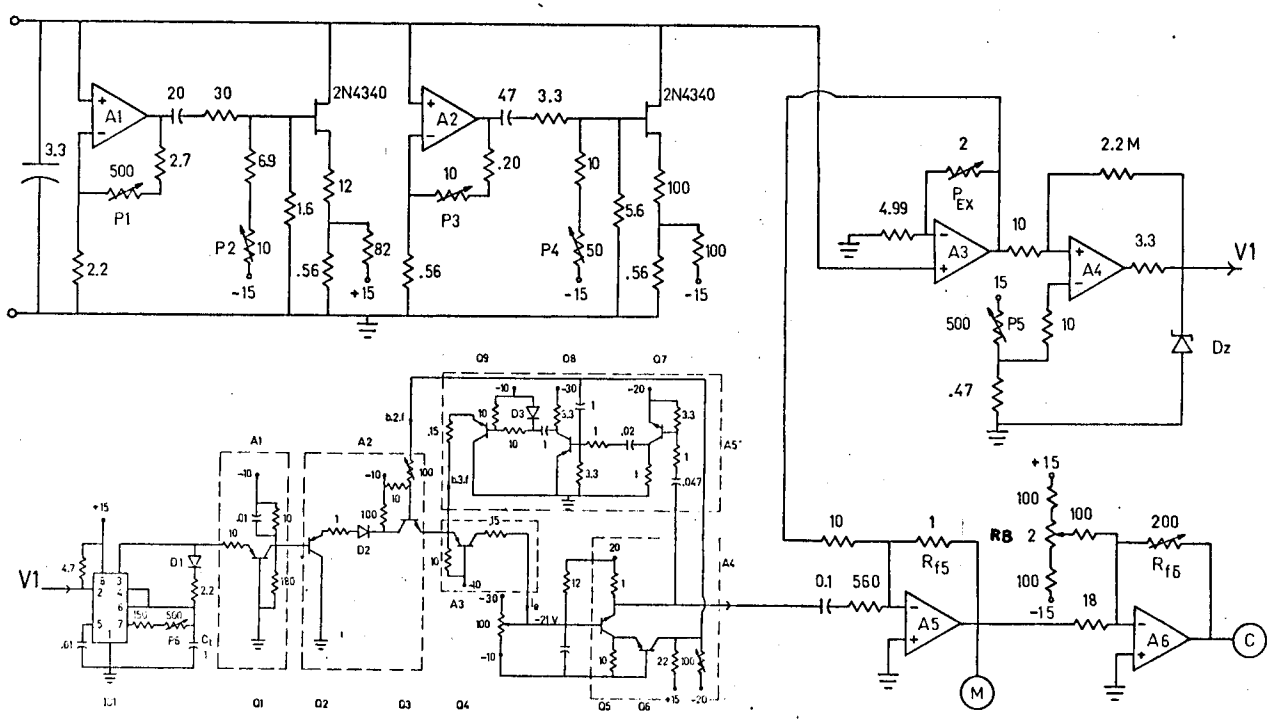

Fig. 10 Electrical diagram of the electronic oscillator used to simulate both the intestinal electrical activities, ECA and ERA. Amplifiers are of type μA741. IC1 is of type NE555. NPN transistors are of type SK3011. PNP transistors are of type SK 3004. D1-D3 are of type 1N4454. Dz is of type 1N758A. All component values are in KΩ and μF unless otherwise indicated.

A5. Due to alterations of the original signal, A6 was also provided with potentiometers denoted by R_B and R_{f_6} for purposes of matching bias and gain of the original signal,respectively. Its output, denoted by C in fig. 10, will be used with experiments of coupling analogs together, as will be seen in chapter 5.

4.2 Experiments with a single oscillator

The analog was built in a card allowing an easy access to each of the potentiometers. It was plugged into a chassis as shown in fig. 11, which will eventually accommodate four such analogs for coupling purposes.

A representative output of the analog's performance as a single unit is shown in figs. 12 and 13 for two different intrinsic frequencies, respectively.

In fig. 12, potentiometer settings P1 to P4 were adjusted for the model to have an intrinsic frequency of about 19 cpm (cycles per minute), as well as potentiometer setting P5 was adjusted so that the threshold voltage (V_{TH}) lay about 6 mV above the maximum depolarized value of the control potential. Under these conditions the model gave an output as shown in the top waveform of fig. 12.

When the magnitude of the control potential was increased, as a result of varying the potentiometer setting P_{ex}, it reached the threshold voltage (V_{TH}) and hence trig-

(a)

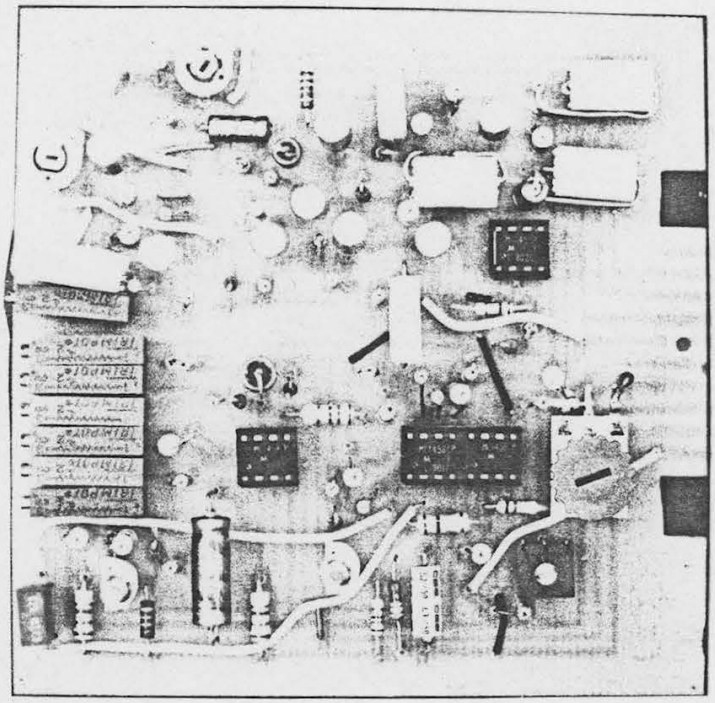

(b)

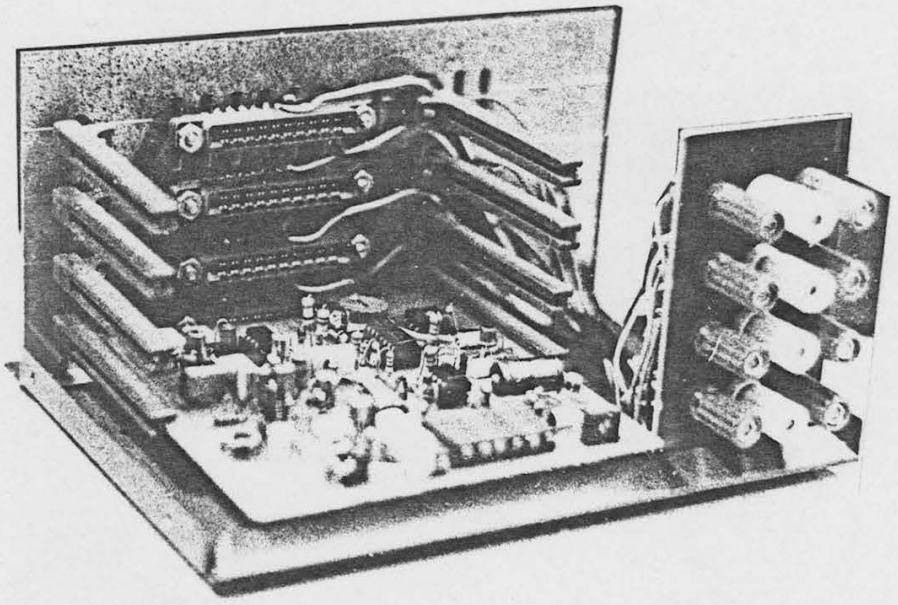

Fig. 11 Shows the electronic analog built in a card (a), and plugged into a chassis (b).

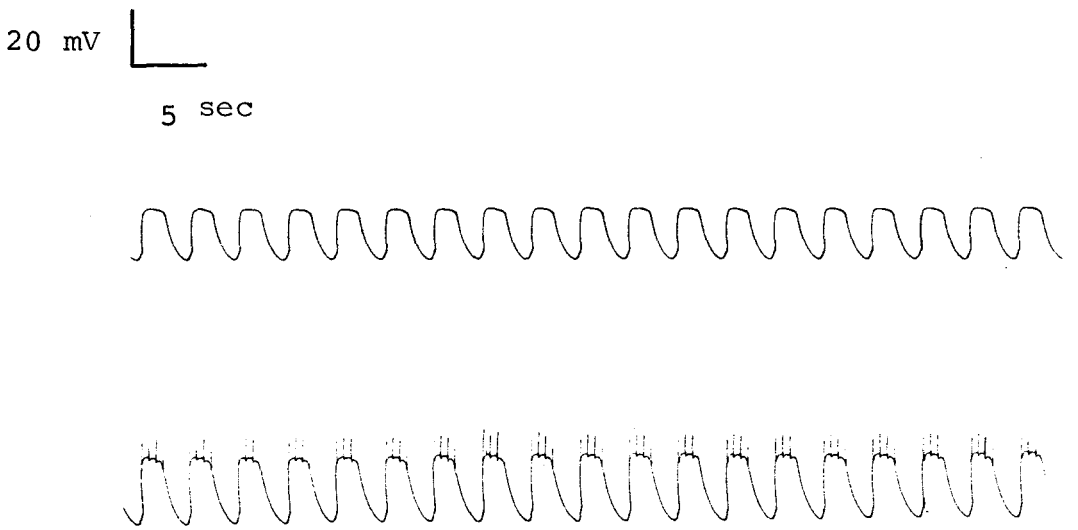

Fig. 12 Waveforms from a single oscillator having a frequency of 19 cpm (top one). By varying potentiometer Pex the magnitude of the control potential was increased and hence response potentials occurred. Calibration marks are valid for all traces.

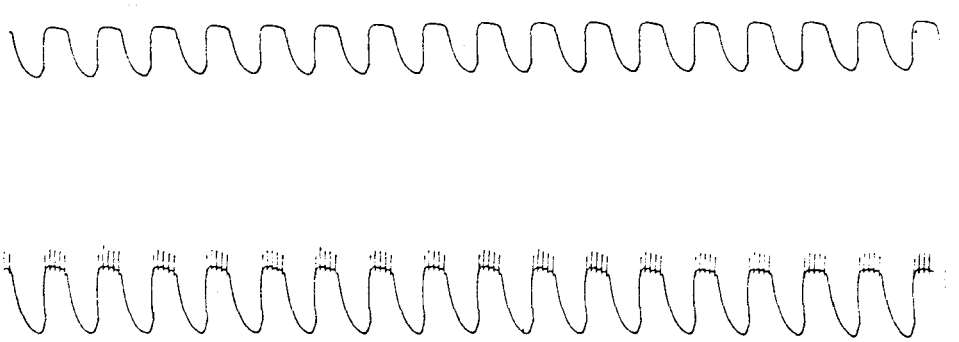

Fig. 13 Waveforms from a single oscillator set to a frequency of 17 cpm. It can be noted that response potentials were also obtained when potentiometer Pex was varied. Calibration marks are same as in fig. 12.

gered the ERA circuit. Accordingly, the appearance of response potentials become apparent as shown in the bottom waveform of fig. 12. This waveform in turn represents the analog's output when both the electrical activities, ECA and ERA, are simulated.

In fig. 13, the analog was set to oscillate at an intrinsic frequency of about 17 cpm, and at a sightly different frequency of response potentials by readjusting potentiometer settings P1 to P6. As a result of this, top and bottom waveforms in fig. 13 represent the analog's output under such conditions. From the bottom waveform, it can be noted the increased amplitude of control potentials, and the appearance of response potentials.

4.3 Results

From the above results it is demonstrated that a single electronic oscillator is capable of qualitatively reproducing two modes of oscillations which may correlate with the small intestinal electrical control and electrical response activities.

It is also demonstrated that when varying the potentiometer setting P_{ex}, which simulates the effect of ACh, the magnitude of control potentials was increased and hence response potentials were observed on top of them. Otherwise, the magnitude of control potentials remained the same and no

response potentials occurred.

Furthermore, it has been suggested that the intestine is a complex of relaxation type oscillators, each of which is capable of oscillating at its own frequency, but can be affected in frequency and phase by the presence of higher and lower frequency oscillators in the neighborhood. Therefore, by choosing appropriate parameter settings, a chain of these electronic oscillators can be set up to give the basic characteristics of the small intestine.

CHAPTER 5

EXPERIMENTS WITH A CHAIN OF OSCILLATORS

A representative set of responses obtainable from a single electronic oscillator by adjusting its parameter potentiometers has been shown in chapter 4. These results illustrated the generic forms of the electronic analog simulating both the electrical control and the electrical response activities in real magnitude and frequency.

In this chapter, four such electronic oscillators are used and arranged in a chain structure to demonstrate frequency entrainment.

5.1 Model characteristics for entrainment

The myogenic electrical oscillations present in the smooth muscle cells of the gastrointestinal tract have been widely likened to relaxation type oscillations, which were originally used to model the biological rhythm in heart muscle. The relaxation oscillators used were of the Van der Pol type or modifications of these, as well as Hodgkin-Huxley type oscillators. These oscillators are distinguished

from linear oscillators (sinusoidal oscillators described by a linear differential equation) and are amenable to modelling the gastrointestinal electrical control activity because when two of these oscillators are coupled, the frequency of oscillation is changed without a major change in their waveform. This permits the frequency of waves to be altered by coupling without interfering with the use of a particular waveform to control a local phenomenon. Thus, the waveform can control the local membrane excitability to occurrence of spikes and contractions in the time domain irrespective of frequency.

This nonlinear characteristic is provided in this electronic analog by the **ECA** circuit, as can be seen from fig. 5 in chapter 3. There it was noted that a necessary condition for oscillations to occur in the ECA circuit was that the currents through the FET's were not equal and opposite. It was also seen that the necessary voltage dependency of the conductances was given by amplified feedback of the voltage between source and ground via operational amplifiers A1 and A2. In addition, by placing capacitors C1 and C2 in these feedback paths, the rapid and slow inactivation time for each FET were provided. Accordingly, the ECA circuit could simulate a threshold potential at which it changes its characteristic and initiates an oscillation; that is, it becomes voltage dependent.

It should not be confused here the term 'threshold potential' with the term 'threshold voltage' , denoted by

V_{TH} , which has been used in previous chapters. While the former is referred to as the voltage at which one oscillator becomes voltage dependent, the latter is referred to as the voltage level that the control potential has to reach for response potentials to occur.

When two of these oscillators having different frequencies of oscillation are coupled together, one oscillator may provide an electrical input to the other oscillator before it reaches its threshold potential and may force its potential to the threshold prematurely or delay it. Furthermore, whether the driving oscillator (having a higher intrinsic frequency than the driven one) can actually drive the other oscillator or not is determined by whether or not the input from it is sufficient to force the potential of lower intrinsic frequency to threshold.

Accordingly, if the input from the higher frequency oscillator will arrive just before the other is ready to oscillate, both the oscillators will oscillate at the same frequency. In other words, they will become entrained or phase locked. However, if the difference in intrinsic frequencies is larger, there will be a larger potential difference between the present value and the threshold potential, and greater input will be required to the threshold, and/or a longer time will ensue before the driven oscillator reaches threshold. In the event the input is insufficient, the second oscillator will not become phase

locked to the high frequency oscillator. The input, however, will shorten the period to the next cycle in some cycles when the potential of the lower frequency oscillator is near threshold; that is, its frequency will be pulled up.

5.2 Bilateral coupling

In all smooth muscle the cells appear to be electrically coupled to one another. The extent of this coupling may vary from one tissue to another, but some coupling has always been detected. This means that any changes in membrane potential of one cell will cause some changes in the membrane potential of all cells around it. Thus, no cell is independent of its neighbors, and the electrical changes in a cell may be related to the electrical activity of hundreds of nearby cells, the nearest ones making the largest contribution. In such a situation, the idea of bilateral coupling where the proximal ones should affect the distal ones and viceversa, seems to be a reasonable assumption.

Forward coupling means that the output of an oscillator is feeding into the next distal oscillator, while backward coupling means that an oscillator is affecting the next proximal oscillator. Therefore, the term bilateral coupling will refer to both of the above mentioned couplings together.

Throughout the experiments, forward and backward

couplings were arranged through potentiometers so that any desired coupling factor could be obtained. In addition, the magnitudes of the two couplings between adjacent oscillators were kept the same as would normally be expected when two cells are in close proximity with one another. The physical analog of this coupling in the intestine may be that a proximal cell is affecting the membrane potential of the next distal cell either by altering its membrane voltage through the cell junction or by setting up currents in the extracellular fluid as a result of potential variations across its membrane.

5.3 Experimental procedure

A chain structure comprising four of these electronic oscillators, as shown in fig. 14, was investigated with various coupling factors, and also when all the four oscillators were not operating in dual mode (ECA and ERA at the same time).

The oscillators were built one to a card and plugged into a chassis which acommodates four cards horizontally allowing access to each of the potentiometers. The chassis has a set of model outputs which allows external connections for any configuration among the oscillators, as well as for monitoring their outputs. Fig. 15 shows a picture of the chassis with the cards.

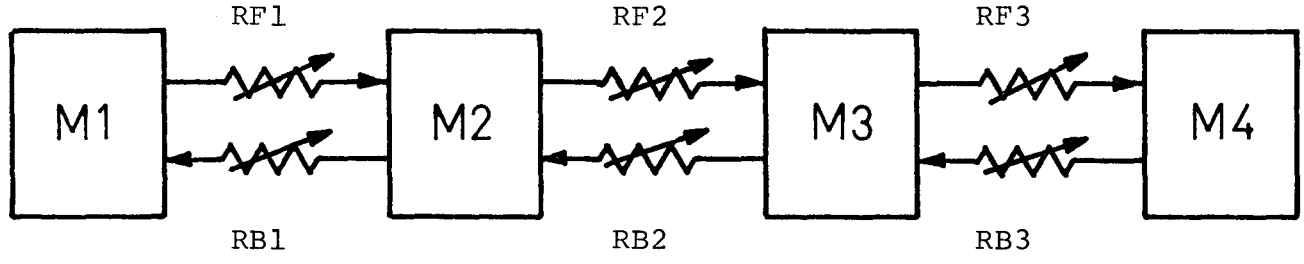

Fig. 14 Block diagram illustrating the arrangement of a chain structure formed with four electronic oscillators. M's denote oscillator numbers. RF's and RB's are potentiometers representing forward and backward coupling factors, respectively.

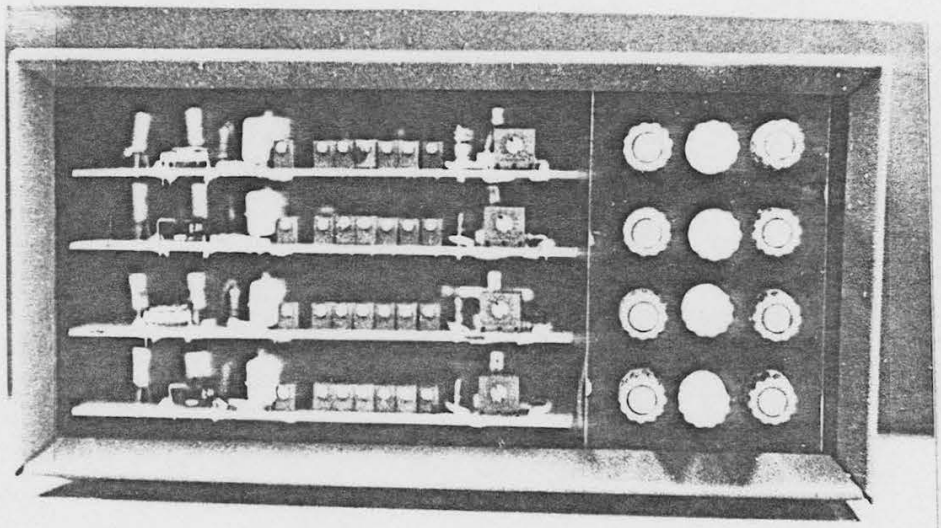

Fig. 15 Shows the chassis with the electronic oscillators plugged into it. They were built one to a card, allowing easy access to each of their potentiometers. The chassis provides a set of outputs to make external connections among oscillators, as well as for monitoring their waveforms.

The oscillators were set to represent two different intrinsic frequency gradients (F1 and F2), as shown in tables I and II below, and then coupling factors were found for frequency entrainment.

The output waveforms were monitored using a storage dual beam oscilloscope 5031 Tektronix, and recorded through an 8-channel Beckman R-611 Dynograph Recorder.

TABLE I

Frequency gradient F1

oscillator number	frequency (cpm)
M1	19.35
M2	18.75
M3	18.18
M4	17.14

TABLE II

Frequency gradient F2

oscillator number	frequency (cpm)
M1	18.63
M2	18.33
M3	18.29
M4	18.02

5.4 Results

When the oscillators were coupled as shown in fig. 14 and operating at a frequency gradient F1 as shown in table I, coupling factors were chosen until the well known intestinal phenomenon of frequency entrainment was obtained. Resistor values of up to almost 1 MΩ provided a satisfactory range of resistive coupling conditions.

Fig. 16 shows the output waveforms recorded from each oscillator in the uncoupled state, and operating in only one mode (ECA). In this and all the following figures the numbers on the right of the traces refer to the oscillator number, and the waveforms always are arranged so that the one at top corresponds to the oscillator having the highest intrinsic frequency, the next below corresponds to the second highest and so on, unless otherwise indicated. Fig. 17 also shows these uncoupled outputs, but with the oscillators operating in dual mode; that is, ECA and ERA are present.

Considering the large frequency gradient between the uncoupled oscillators, two sets of resistive coupling values were chosen for observing the effects of coupling. The first set of values was considered as a 'weak coupling', while the second was considered as a 'strong coupling'. The list of these values is given in table III below. Coupling factors are denoted by R's (see also fig. 14), where RF and RB indicate forward and backward couplings, respectively.

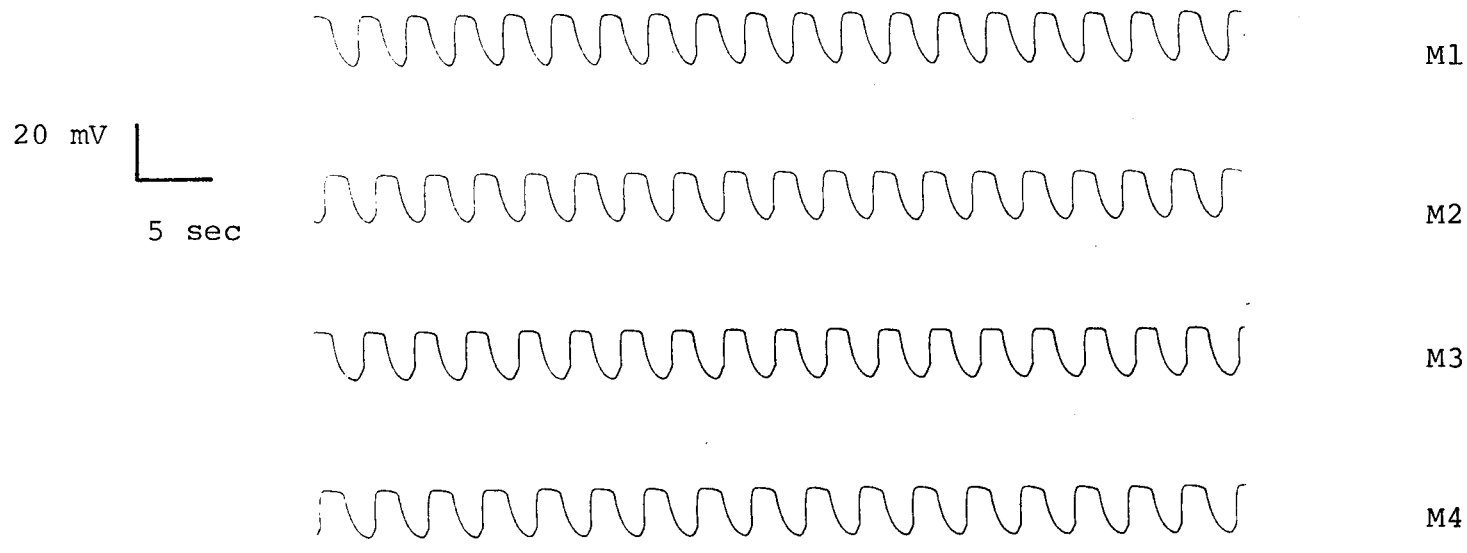

Fig. 16 Oscillators adjusted to have uncoupled frequencies (according to the frequency gradient F1) and operating in only one mode (ECA). In this and all the following figures the numbers on the right of the traces refer to the oscillator number, and calibration marks are valid for all traces.

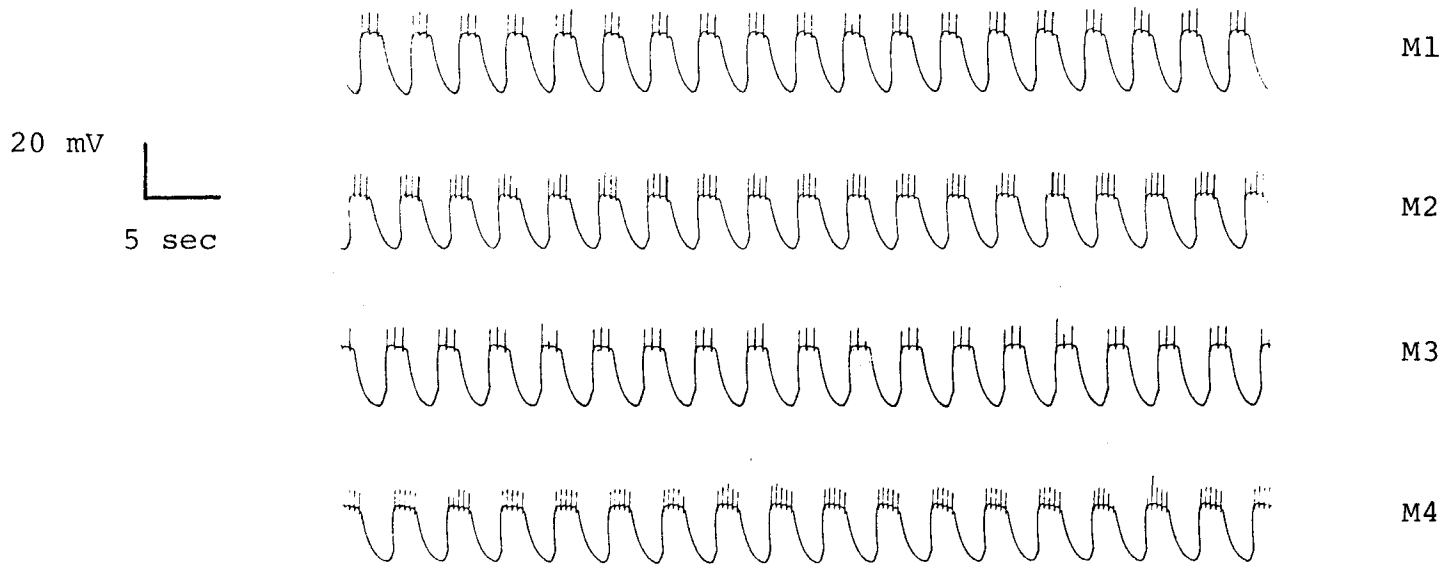

Fig. 17 Oscillators adjusted to have uncoupled frequencies (according to the frequency gradient F1) and operating in dual mode (ECA and ERA).

TABLE III

Resistive values of coupling factors used for frequency gradient F1

'weak coupling'

coupling factor	resistive value (KΩ)
RF1 = RB1	730
RF2 = RB2	405
RF3 = RB3	274

'strong coupling'

coupling factor	resistive value (KΩ)
RF1 = RB1	130
RF2 = RB2	210
RF3 = RB3	250

Figs. 18 and 19 show the output waveforms when the oscillators were weakly coupled, and operating in one and two modes respectively. When the coupling strength between oscillators was increased, a stronger coordinated effect was apparent as shown in fig. 20 for one mode, and in fig. 21 for dual mode.

The resultant waveforms in figs. 18 to 21 show frequency entrainment considering both, weak and strong, coupling factors at a frequency approximately the same as the higher intrinsic frequency of oscillator M1. It should also be noted from these results that the waveforms were not

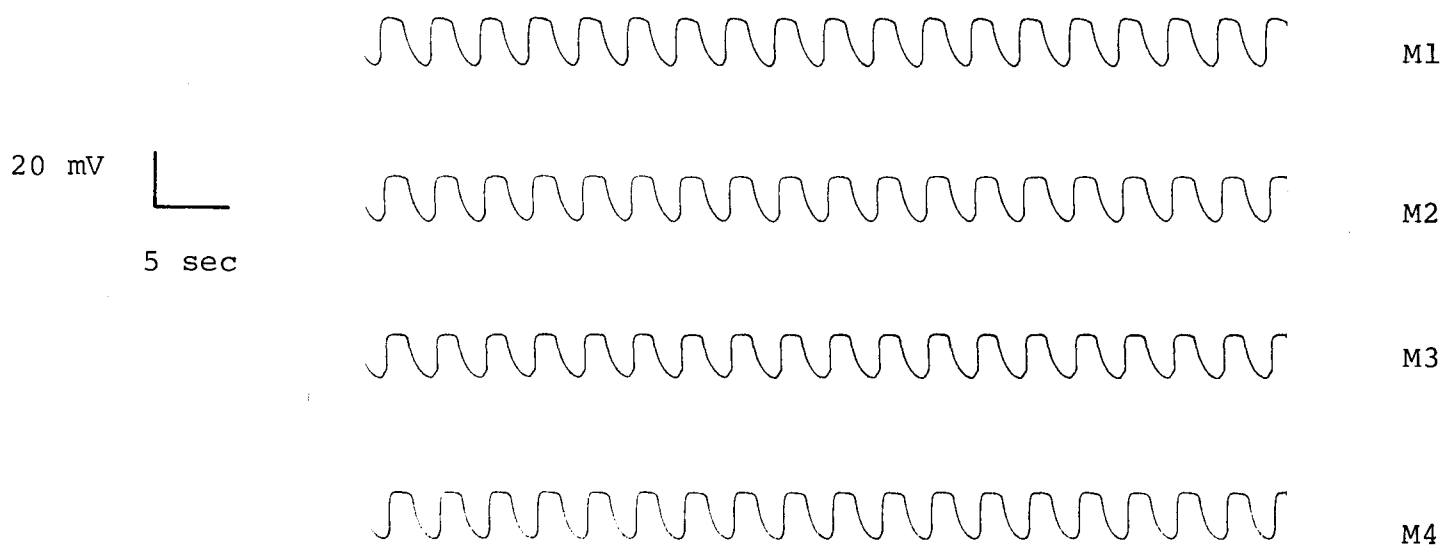

Fig. 18 Typical waveforms from oscillators 'weakly' coupled, and operating in the ECA mode. In the uncoupled state they were oscillating at a frequency gradient F1.

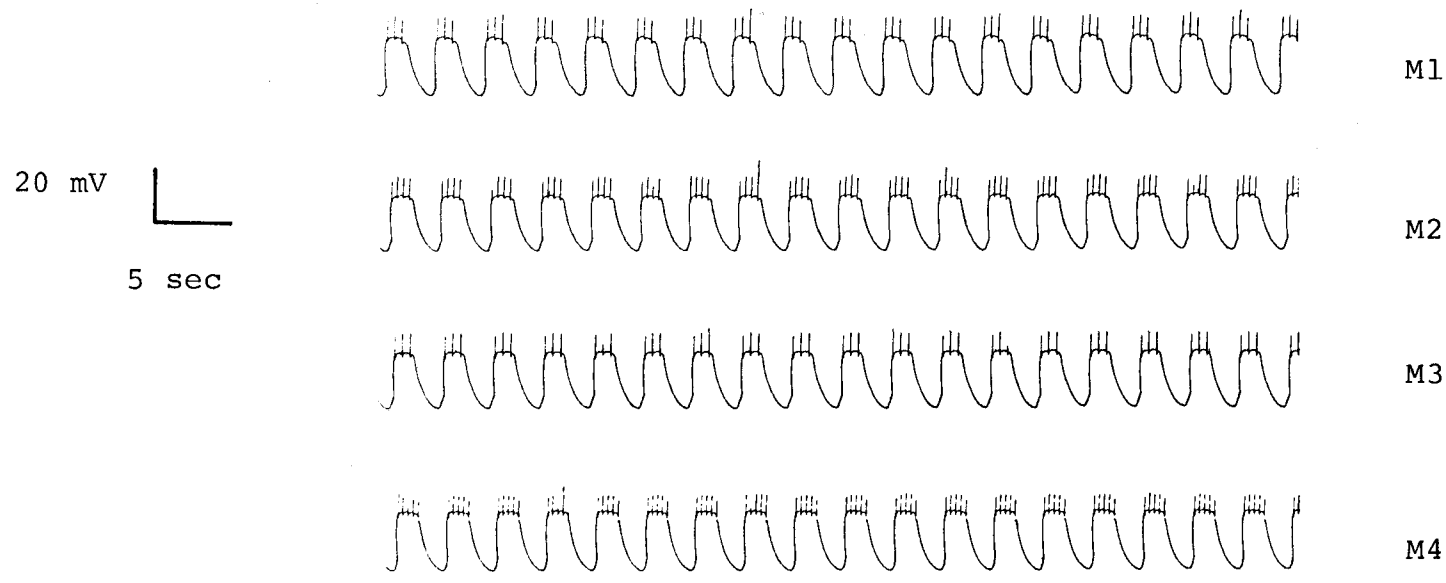

Fig. 19 Typical waveforms from oscillators 'weakly' coupled, and operating in dual mode (ECA and ERA). In the uncoupled state they were oscillating at a frequency gradient F1.

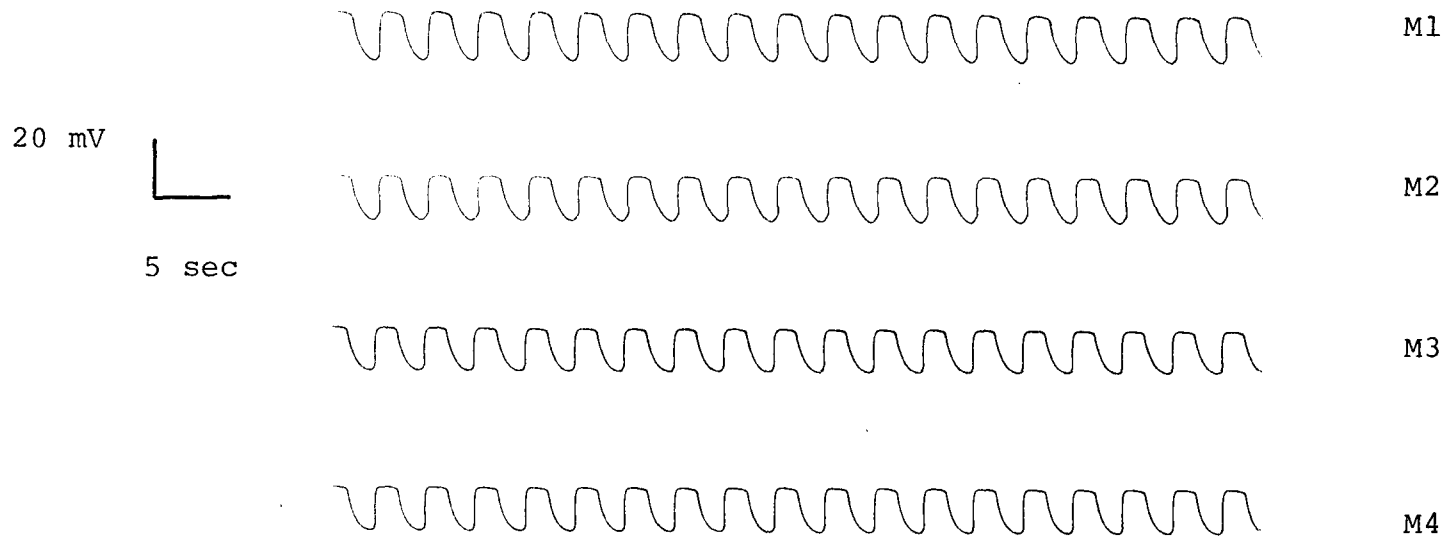

Fig. 20 Shows typical waveforms when the oscillators were 'strongly' coupled, and operating in only one mode (ECA). They were adjusted at a frequency gradient F1 in the uncoupled state.

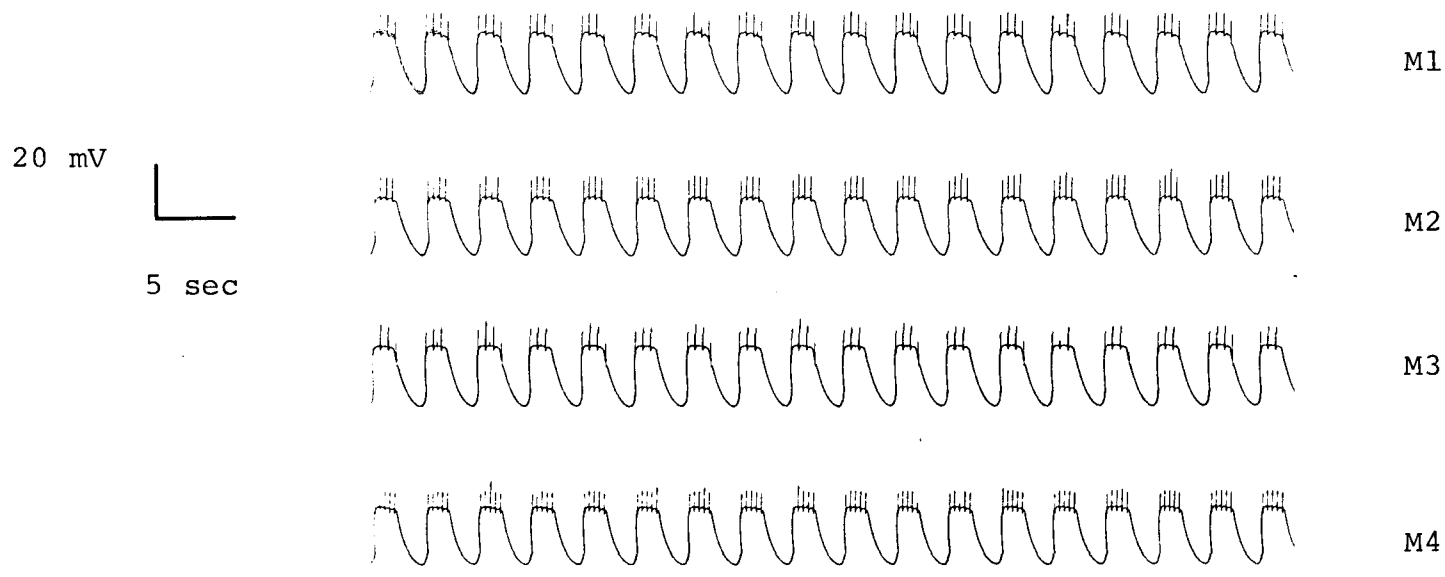

Fig. 21 Shows typical waveforms when the oscillators were 'strongly' coupled, and operating in dual mode (ECA and ERA, simultaneously). They were adjusted at a frequency gradient F1 in the uncoupled state.

affected by coupling, even when the oscillators were operating in dual mode. Furthermore, fig. 22 which shows an expanded version of the output waveforms for weak and strong coupling factors demonstrates that the oscillators were very easily entrained, even when a large frequency gradient and relatively weak coupling were present. It can also be noted from fig. 22 the marked difference in phase shifts between oscillators due to the strength of coupling factors.

The oscillators were also used to investigate the behavior of the chain when the intrinsic frequency gradient was made smaller than the one denoted by F1 in table I. A new set of intrinsisc frequencies denoted by F2 in table II was selected, and the oscillators were coupled as shown in fig. 14.

Under this situation, the effect of coupling was demonstrated by selecting a new set of 'weak' and 'strong' resistive coupling factors, as listed in table IV below. Also in this case the oscillators were set to operate in dissimilar modes; that is, not all of them were in dual mode.

Fig. 23 shows the output waveforms of uncoupled oscillators. It should be noted here that oscillators M2 and M4 were operating in dual mode, whereas oscillators M1 and M3 were in a single mode.

Figs. 24 and 25 show the output waveforms corresponding to a weak and strong coupling factors, respectively. Fig. 26 shows an expanded version of the waveforms due to

these two coupling factors.

The resultant waveforms in this case also show that the driven oscillators M2, M3, and M4, are entrained at approximately the frequency of oscillation of the driving oscillator M1. In addition, it is also seen that the waveforms were not affected by the coupling of oscillators in dissimilar modes. It thus appears that coupling oscillators in dissimilar modes does correlate with physiological data in which the frequency of control potentials is not changed at all in the presence of response potentials.

TABLE IV

Resistive values of coupling factors used for frequency gradient F2

'weak coupling'

coupling factor	resistive value (KΩ)
RF1 = RB1	690
RF2 = RB2	770
RF3 = RB3	638

'strong coupling'

coupling factor	resistive value (KΩ)
RF1 = RB1	205
RF2 = RB2	200
RF3 = RB3	150

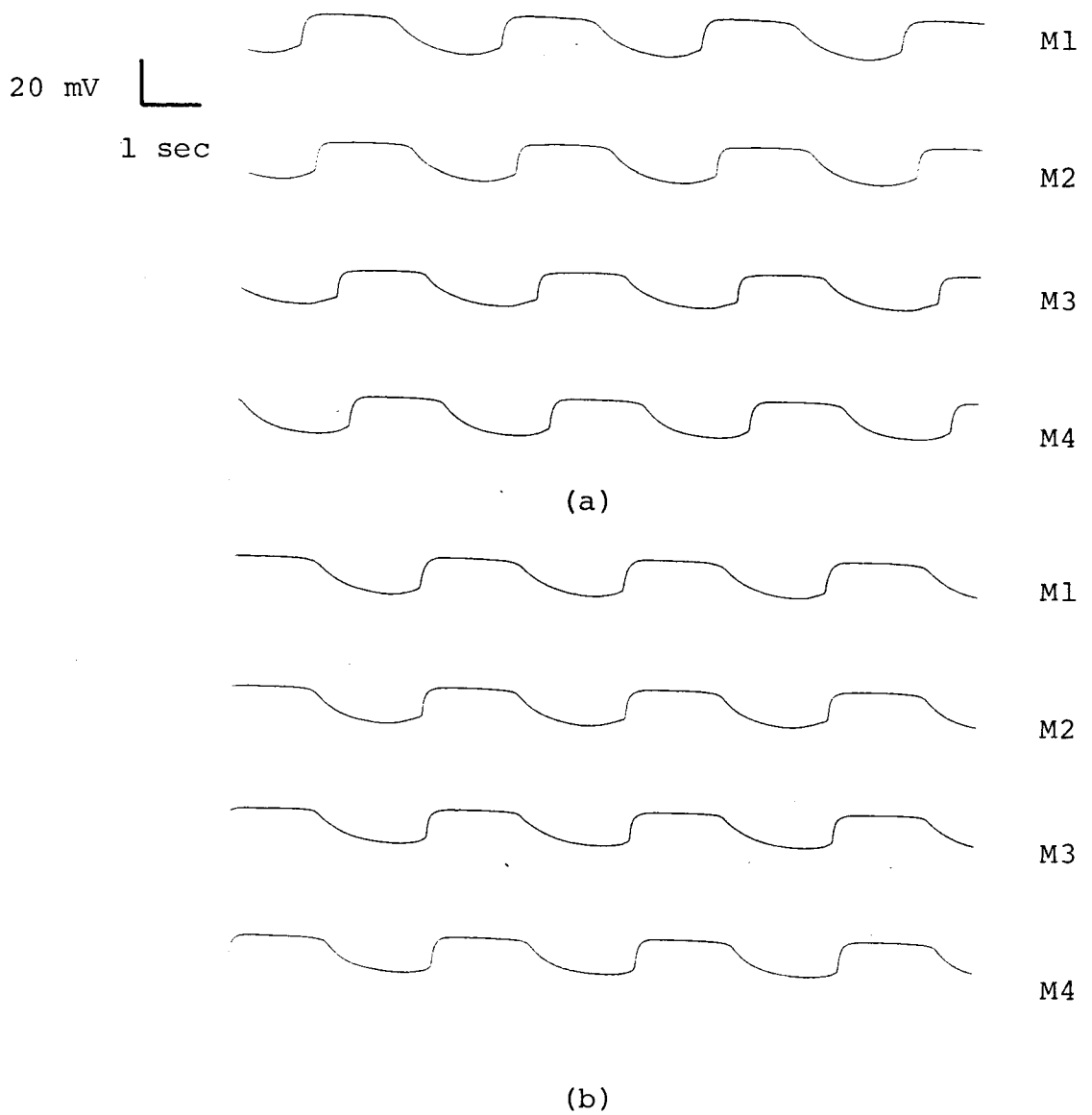

Fig. 22 Shows an expanded version of the waveforms from coupled oscillators operating in the ECA mode. (a) for a 'weak' coupling. (b) for a 'strong' coupling. It can be noted the marked difference in phase shifts between oscillators when the strength of coupling is increased. Calibration marks are valid for all traces.

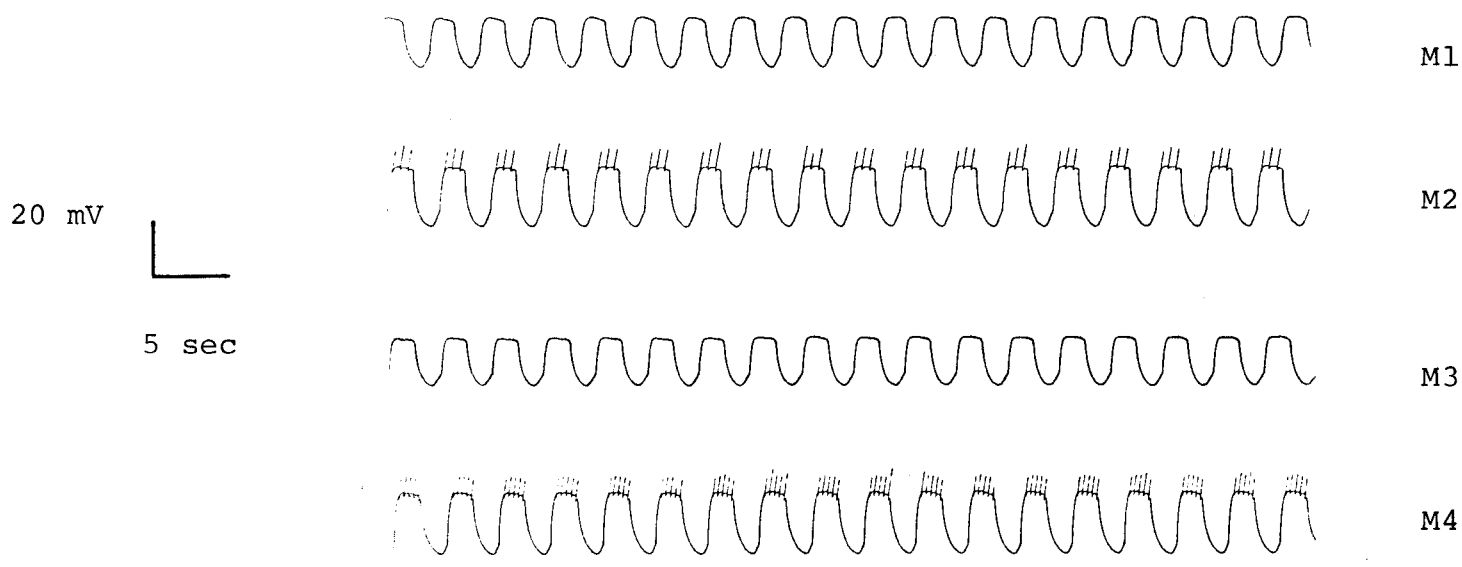

Fig. 23 Shows waveforms from oscillators operating in dissimilar modes. They are in the uncoupled state and adjusted to oscillate at a frequency gradient F2.

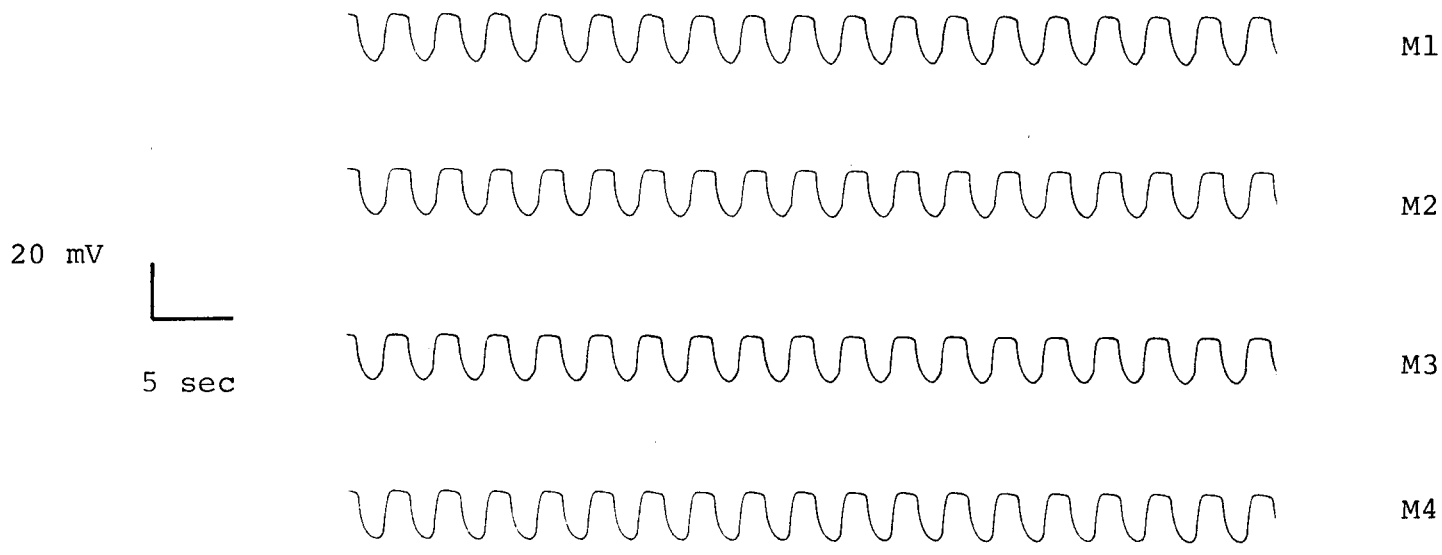

Fig. 24 Typical waveforms from oscillators 'weakly' coupled, and operating in only one mode. In the uncoupled state they were adjusted to oscillate at a frequency gradient F2.

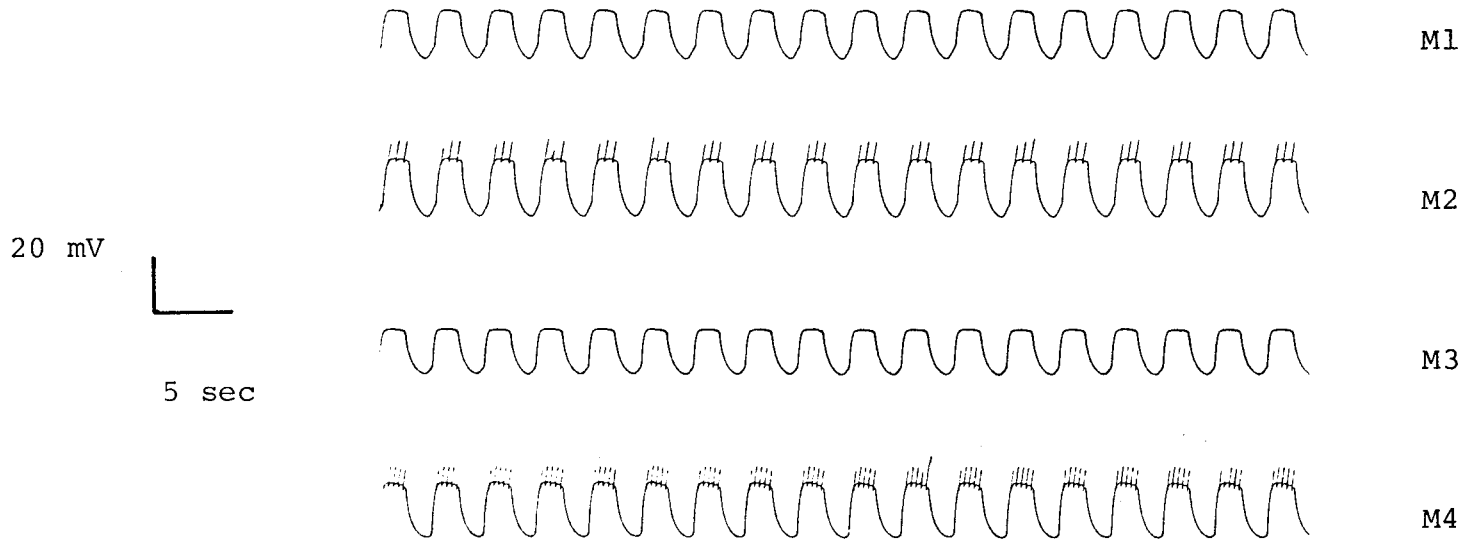

Fig. 25 Shows waveforms from oscillators 'strongly' coupled, and operating in dissimilar modes. In the uncoupled state they were adjusted to oscillate at a frequency gradient F2.

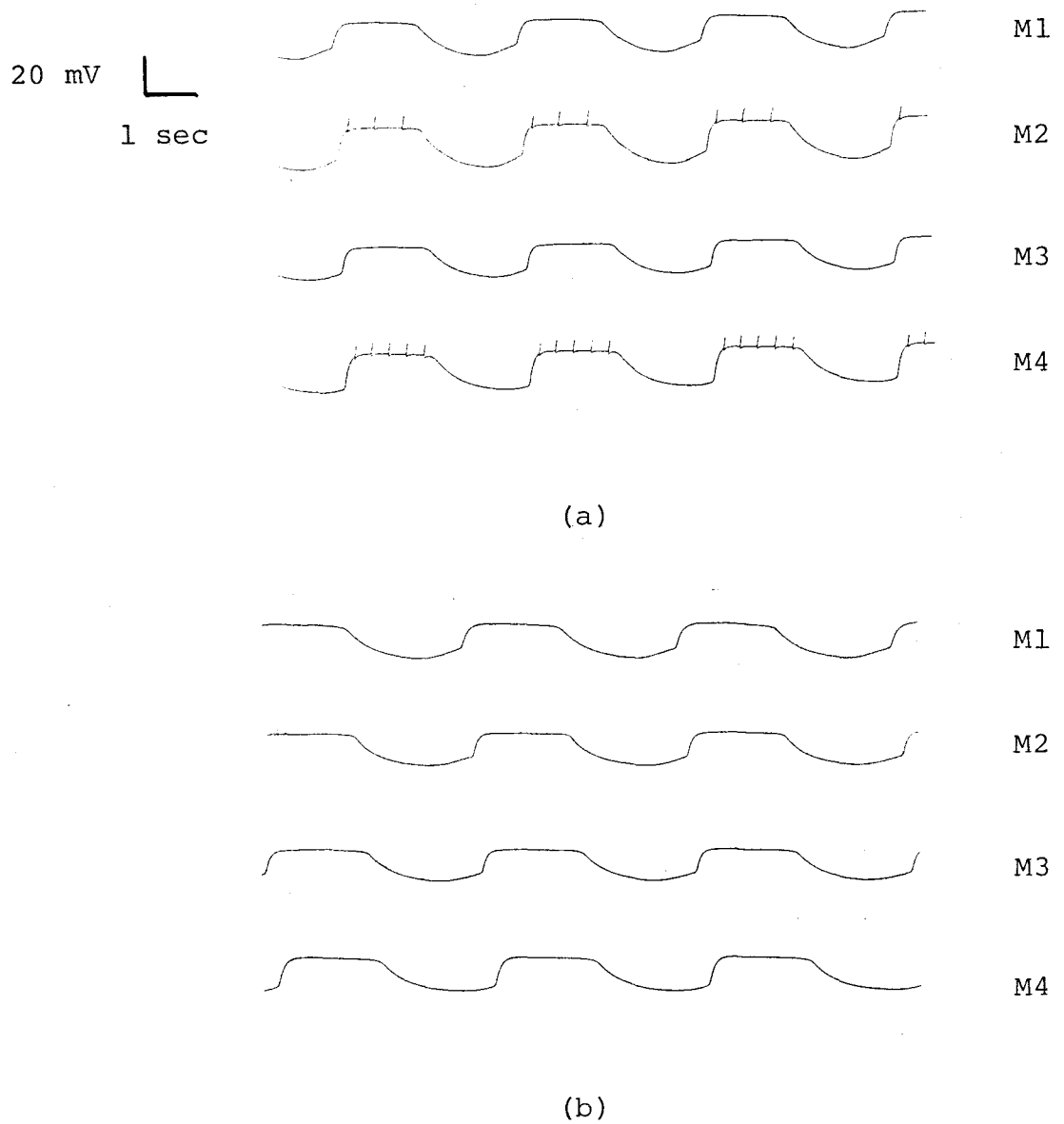

Fig. 26 Shows an expanded version of the waveforms from coupled oscillators. (a) for a strong coupling factor and operating in dissimilar mode. (b) for a weak coupling factor and operating in one mode. Calibration marks are valid for all traces.

CHAPTER 6

CONCLUSIONS

It has been demonstrated that the proposed electronic oscillator is capable of qualitatively reproducing, in real frequency and magnitude, both the electrical activities present in the small intestine, ECA and ERA.

In addition, a chain of four of these bidirectionally coupled electronic analogs have been used to reproduce the well known entrainment phenomena, and to show that the capability of these oscillators to entrain others strongly depends upon the intrinsic frequencies of the coupled oscillators, as well as upon the amount of coupling available.

The results obtained also show that it could not be very difficult that by choosing appropriate intrinsic frequencies and coupling factors, a chain of these electronic oscillators can be set up to give the electrical pattern found in the small intestine. Furthermore, on the basis of the observed performance of the network, some new hypothesis or conditions might be put forward for a better understanding of electrical activities in the small intestine.

On the other hand, even when the electronic analog

is not fully described in terms of the Hodgkin-Huxley dynamics because of the incomplete knowledge of the membrane ionic mechanisms in smooth muscle cells, it still has some interesting approaches which make it more convenient for simulating gastrointestinal electrical activities than by using other modelling attempts based on digital simulations.

One of the drawbacks of digital modelling is the very long computing time required for simulating even a few oscillators and a small number of oscillation periods. Another disadvantage of this digital simulation is that it prevents effective use of one of our most valuable analytical tools, our eyes.

There is considerable advantage to observing real time data while stimuli and model parameters are changed. Direct observations of waveforms, phase relationships, and time dependent interactions are revealing and suggestive. This is especially true in an interdisciplinary research environment where this type of modelling acts as a better vehicle and provides motivation for obtaining more accurate information about smooth muscle parameters, as in this case.

Further useful applications of the electronic analog will be possible when the ionic mechanisms underlaying the smooth muscle cell membrane are unravelled.

REFERENCES

Alvarez W. C. (1940). An introduction to Gastroenterology. P. B. Hoeber, Inc., New York.

Abe Y. and T. Tomita (1968). Cable properties of smooth muscle. J. Physiol., 196 : 87-100.

Bass P. (1965). Electrical activity of smooth muscle of the gastrointestinal tract. Gastroenterology, 49 : 391-394.

Bortoff A. (1961). Slow potential variations of small intestine. Am. J. Physiol., 201 : 203-208.

Bozler E. (1938). The action potentials of visceral smooth muscle. Am. J. Physiol., 124 : 502-510.

Bozler E. (1946). The relation of the action potentials to mechanical activity in intestinal muscle. Am. J. Physiol., 146 : 496-501.

Brown B. H., K. K. Ng. K. Kwong, H. L. Duthie, G. E. Whittaker and C. I. Franks (1971). Computer analysis and simulation of human gastroduodenal electrical activity. Med. Biol. Eng., 9 : 305-314.

Brown B., H. L. Duthie, A. R. Horn and R. H. Smallwood (1975). A linked oscillator model of electrical activities of human small intestine. Am. J. Physiol., 229 : 384-388.

Bulbring E. and I. N. Hooton (1954). Memebrane potential of smooth muscle fibers in the rabbit's sphincter

pupillae. J. Physiol., 125 : 292-301.

Burnstock G., M. E. Holman and C. L. Prosser (1963). Electrophysiology of smooth muscle. Physiol. Rev., 43 : 482-527.

Daniel E. E., D. R. Carlow, B. T. Wachter, W. H. Sutherland and A. Bogoch (1959). Electrical activity of the small intestine. Gastroenterology, 37 : 268-281.

Daniel E. E., A. J. Honour and A. Bogoch (1960). Electrical activity on the longitudinal muscle of dog small intestine studied in vivo using microelectrodes. Am. J. Physiol., 198 : 113-118.

Daniel E. E., B. T. Wachter, A. J. Honour and A. Bogoch (1960). The relationship between electrical and mechanical activity of the small intestine of dog and man. Can. J. Biochem. Physiol., 38 : 777-801.

Daniel E. E. and K. M. Chapman (1963). Electrical activity of the gastrointestinal tract as an indication of mechanical activity. Am. J. Digest. DIS., 8 : 54-102.

Diamant N. E., P. K. Rose and E. J. Davison (1970). Computer simulation of intestinal slow wave frequency gradient. Am. J. Physiol., 219 : 1684-1690.

Duthie H. L. (1974). Electrical activity of the gastrointestinal smooth muscle. GUT, 15 : 669-681.

Gulrajani R. M. and F. A. Roberge (1976). The modelling of the Hodgkin-Huxley membrane with field-effect tran-

transistor analog. Biol. Cyber., 25 : 227-240.

Hodgkin A. L. and A. F. Huxley (1952.a). Currents carried by sodium and potassium ions through the membrane of the giant axon of Loligo. J. Physiol., 116 : 449-472.

Hodgkin A. L. and F. A. Huxley (1952.b). The components of membrane conductance in the giant axon of Loligo. ibid., 116 : 473-496.

Hodgkin A. L. and F. A. Huxley (1952.c). The dual effect of membrane potential on sodium conductance in the giant axon of Loligo. ibid., 116 : 497-506.

Hodgkin A. L. and F. A. Huxley (1952.d). A quantitative description of membrane current and its application to conduction and excitation in nerve. ibid., 117 : 500-544.

Holaday D. H., H. Volk and J. Mandell (1958). Electrical activity of the small intestine with special reference to the origin of rhythmicity. Am. J. Physiol., 195 : 505-515.

Kobayashi M., T. Nagai and C. L. Prosser (1966). Electrical interaction between muscle layers of cat intestine. Am. J. Physiol., 211 : 1281-1291.

Kobayashi M., C. L. Prosser and T. Tomita (1967). Electrical properties of smooth muscle as measured intracellular and extracellularly. Am. J. Physiol., 213 : 275-286.

Lewis E. R. (1968). An electronic model of neuroelectric

point processes. Kybernetik, 5 : 30-46.

Linkens D. A. and S. P. Datardina (1977). Frequency entrainment of coupled Hodgkin-Huxley type oscillators for modelling gastrointestinal electrical activity. I.E.E.E. Trans., BME-24 : 362-365.

Linkens D. A. (1980). Electronic modelling of slow waves and spike activity in intestinal tissue. I.E.E.E. Trans., BME-27 : 351-357.

Milton G. W. and A. W. M. Smith (1956). The pacemaking area of the duodenum. J. Physiol., 132 : 100-114.

Nagai T and C. L. Prosser (1963). Electrical parameters of smooth muscle cells. Am. J. Physiol., 204 : 915-924.

Nelson T. S. and J. C. Becker (1968). Simulation of the electrical and mechanical gradient of the small intestine. Am. J. Physiol., 214 : 749-757.

Patton R. J. and D. A. Linkens (1977). Phenomenological investigation of a distributed parameter model for coordinating the mechanical activity of the mammalian gut. In IFAC 2nd Symp. Contr. Distributed Parameter Syst., Univ. Warwick, Warwick, England. pp. 1-17.

Patton R. J. and D. A. Linkens (1978). Hodgkin-Huxley type electronic modelling of gastrointestinal activity. Med. Biol. Eng. and Comput., 16 : 195-202.

Puestow C. B. (1933). Studies on the origin of the automaticity of the intestine: the action of certain drugs

on isolated intestinal.transplants. Am. J. Physiol. 106 : 682-688.

Roy G. (1972). A simple electronic analog of the squid axon membrane: the Neurofet. I.E.E.E. Trans., BME-19 : 60-63.

Robertson-Dunn V. and D. A. Linkens (1974). A mathematical model of the slow wave electrical activity of the human small intestine. Med. Biol. Eng., 214 : 750-757.

Sarna S. K., E. E. Daniel and Y. J. Kingma (1971). Simulation of slow wave electrical activity of the small intestine. Am. J. Physiol., 221 : 166-175.

Sarna S. K. (1975). Gastrointestinal electrical activity: Terminology. Gastroenterology, 68 : 1631-1635.

Taher Y. El-Sharkawy and E. E. Daniel (1975). Ionic mechanisms of intestinal electrical control activity. Am. J. Physiol., 229 : 1287-1298.

Van der Pol V. and Van der Mark J. (1928). The heart beat considered as a relaxation oscillator and a electrical model of the heart. Phil. Mag. Suppl., 6 : 763-775.

Guyton A. C. (1977). Basic Human Physiology: normal function and mechanisms of disease. W. B. Sanders Co.

Jung W. G. IC op-amp Cookbook. SAMS publication.

Millman J. and C. C. Halkias (1972). Integrated Electronics: Analog and Digital circuits and systems. Mc Graw-Hill.

Process 52

2N4338-41 N-Channel JFETs

General Description

The 2N4338 thru 2N4341 series of N-channel JFETs is characterized for low to medium frequency amplifier applications. Tight selections of $V_{GS(off)}$, I_{DSS}, g_{fs} results in consistent characteristics in all applications.

Absolute Maximum Ratings (25°C)

Gate-Drain or Gate-Source Voltage	−50V
Gate Current	50 mA
Total Device Dissipation, T_A = 25°C (Derate 2 mW/°C to +175°C)	300 mW
Storage Temperature Range	−65°C to +200°C
Maximum Operating Temperature	175°C
Lead Temperature (1/16" from case for 10 seconds)	300°C

TO-18 2N Series

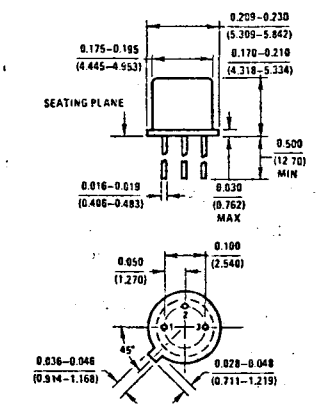

PIN	FET
1	S
2	D
3	G

Electrical Characteristics (25°C unless otherwise specified)

PARAMETER		CONDITIONS		2N4338		2N4339		2N4340		2N4341		UNITS
				MIN	MAX	MIN	MAX	MIN	MAX	MIN	MAX	
I_{GSS}	Gate Reverse Current	V_{GS} = −30V, V_{DS} = 0			−0.1		−0.1		−0.1		−0.1	nA
			150°C		−0.1		−0.1		−0.1		−0.1	μA
BV_{GSS}	Gate-Source Breakdown Voltage	I_G = −1 μA, V_{DS} = 0		−50		−50		−50		−50		V
$V_{GS(off)}$	Gate-Source Cutoff Voltage	V_{DS} = 15V, I_D = 0.1 μA		−0.3	−1	−0.6	−1.8	−1	−3	−2	−6	
$I_{D(off)}$	Drain Cutoff Current	V_{DS} = 15V V_{GS} = ( )			0.05 (−5)		0.05 (−5)		0.05 (−5)		0.07 (−10)	nA (V)
I_{DSS}	Saturation Drain Current	V_{DS} = 15V, V_{GS} = 0		0.2	0.6	0.5	1.5	1.2	3.6	3	9	mA
g_{fs}	Common-Source Forward Transconductance	V_{DS} = 15V, V_{GS} = 0	f = 1 kHz	600	1800	800	2400	1300	3000	2000	4000	μmho
g_{os}	Common-Source Output Conductance				5		15		30		60	
r_{ds}	Drain-Source ON Resistance	V_{DS} = 0, V_{GS} = 0			2500		1700		1500		800	Ω
C_{iss}	Common-Source Input Capacitance	V_{DS} = 15V, V_{GS} = 0	f = 1 MHz		7		7		7		7	pF
C_{rss}	Common-Source Reverse Transfer Capacitance				3		3		3		3	
NF	Noise Figure	V_{DS} = 15V, V_{GS} = 0 R_{gen} = 1M, BW = 200 Hz	f = 1 kHz		1		1		1		1	dB

Low Power Ge Transistors

		NPN SK3011	PNP SK3004
P_T	(Watts)	0.15	0.60
I_C	(Amps)	0.10	-1.0
V_{CB0}	(Volts)	25	-32
V_{CE0}	(Volts)	25	-25
V_{EB0}	(Volts)	12	-12
f_{FE}		70	90
f_T	(MHz)	8	1

signetics TIMER | 555

LINEAR INTEGRATED CIRCUITS

DESCRIPTION

The NE/SE 555 monolithic timing circuit is a highly stable controller capable of producing accurate time delays, or oscillation. Additional terminals are provided for triggering or resetting if desired. In the time delay mode of operation, the time is precisely controlled by one external resistor and capacitor. For a stable operation as an oscillator, the free running frequency and the duty cycle are both accurately controlled with two external resistors and one capacitor. The circuit may be triggered and reset on falling waveforms, and the output structure can source or sink up to 200mA or drive TTL circuits.

FEATURES

- TIMING FROM MICROSECONDS THROUGH HOURS
- OPERATES IN BOTH ASTABLE AND MONOSTABLE MODES
- ADJUSTABLE DUTY CYCLE
- HIGH CURRENT OUTPUT CAN SOURCE OR SINK 200mA
- OUTPUT CAN DRIVE TTL
- TEMPERATURE STABILITY OF 0.005% PER °C
- NORMALLY ON AND NORMALLY OFF OUTPUT

APPLICATIONS

PRECISION TIMING
PULSE GENERATION
SEQUENTIAL TIMING
TIME DELAY GENERATION
PULSE WIDTH MODULATION
PULSE POSITION MODULATION
MISSING PULSE DETECTOR

PIN CONFIGURATIONS (Top View)

T PACKAGE

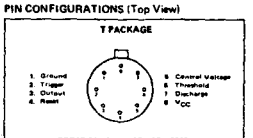

ORDER PART NOS. SE555T/NE555T

V PACKAGE

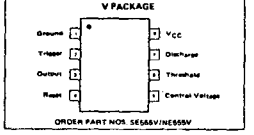

ORDER PART NOS. SE555V/NE555V

ABSOLUTE MAXIMUM RATINGS

Supply Voltage	+18V
Power Dissipation	600 mW
Operating Temperature Range	
NE555	0°C to +70°C
SE555	−55°C to +125°C
Storage Temperature Range	−65°C to +150°C
Lead Temperature (Soldering, 60 seconds)	+300°C

BLOCK DIAGRAM

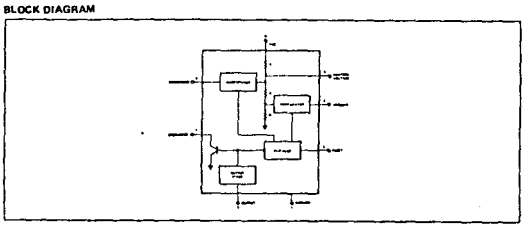

SIGNETICS TIMER • 555

ELECTRICAL CHARACTERISTICS T_A = 25°C, V_{CC} = +5V to +15 unless otherwise specified

PARAMETER	TEST CONDITIONS	SE 555			NE 555			UNITS
		MIN	TYP	MAX	MIN	TYP	MAX	
Supply Voltage		4.5		18	4.5		16	V
Supply Current	V_{CC} = 5V, R_L = ∞		3	5		3	6	mA
	V_{CC} = 15V, R_L = ∞		10	12		10	15	mA
	Low State, Note 1							
Timing Error(Monostable)	R_A, R_B = 1KΩ to 100KΩ							
	Initial Accuracy		0.5	2		1		%
	Drift with Temperature		30	100		50		ppm/°C
	Drift with Supply Voltage		0.05	0.2		0.1		%/Volt
Threshold Voltage			2/3			2/3		× V_{CC}
Trigger Voltage	V_{CC} = 15V	4.8	5	5.2		5		V
	V_{CC} = 5V	1.45	1.67	1.9		1.67		V
Trigger Current			0.5			0.5		µA
Reset Voltage		0.4	0.7	1.0	0.4	0.7	1.0	V
Reset Current			0.1			0.1		mA
Threshold Current	Note 3		0.1	.25		0.1	.25	µA
Control Voltage Level	V_{CC} = 15V	9.6	10	10.4	9.0	10	11	V
	V_{CC} = 5V	2.9	3.33	3.8	2.6	3.33	4	V
Output Voltage (low)	V_{CC} = 15V							
	I_{SINK} = 10mA		0.1	0.15		0.1	.25	V
	I_{SINK} = 50mA		0.4	0.5		0.4	.75	V
	I_{SINK} = 100mA		2.0	2.2		2.0	2.5	V
	I_{SINK} = 200mA		2.5			2.5		
	V_{CC} = 5V							
	I_{SINK} = 8mA		0.1	0.25				V
	I_{SINK} = 5mA					.25	.35	
Output Voltage Drop (low)								
	I_{SOURCE} = 200mA		12.5			12.5		
	V_{CC} = 15V							
	I_{SOURCE} = 100mA							
	V_{CC} = 15V	13.0	13.3		12.75	13.3		V
	V_{CC} = 5V	3.0	3.3		2.75	3.3		V
Rise Time of Output			100			100		nsec
Fall Time of Output			100			100		nsec

NOTES

1. Supply Current when output high typically 1mA less.
2. Tested at V_{CC} = 5V and V_{CC} = 15V.
3. This will determine the maximum value of R_A + R_B for 15V operation, the max total R = 20 megohms.

EQUIVALENT CIRCUIT (Shown for One Side Only)

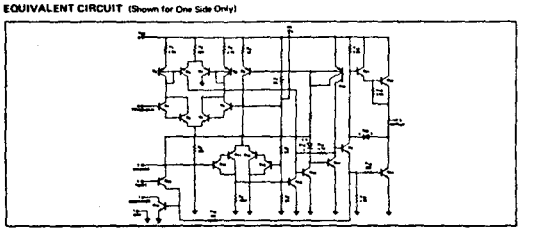

Operational Amplifiers

High-Gain Single and Dual Operational Amplifiers
For Military, Industrial and Commercial Applications

The RCA-CA1458, CA1558 (dual types); CA741C, CA741 (single-types); CA747C, CA747 (dual types); and CA748C, CA748 (single types) are general-purpose, high-gain operational amplifiers for use in military, industrial, and commercial applications.

These monolithic silicon integrated-circuit devices provide output short-circuit protection and latch-free operation. These types also feature wide common-mode and differential-mode signal ranges and have low-offset voltage nulling capability when used with an appropriately valued potentiometer. A 5-megohm potentiometer is used for offset nulling types CA748C, CA748 (See Fig. 10); a 10 kilohm potentiometer is used for offset nulling types CA741C, CA741, CA747CE, CA747CG, CA747E, CA747G (See Fig. 9); and types CA1458, CA1558, CA747CT, have no specific terminals for offset nulling. Each type consists of a differential-input amplifier that effectively drives a gain and level-shifting stage having a complementary emitter-follower output.

This operational amplifier line also offers the circuit designer the option of operation with internal or external phase compensation.

Types CA748C and CA748, which are externally phase compensated (terminals 1 and 8) permit a choice of operation for improved bandwidth and slew-rate capabilities. Unity gain with external phase compensation can be obtained with a single 30-pF capacitor. All the other types are internally phase-compensated.

RCA's manufacturing process makes it possible to produce IC operational amplifiers with low-burst ("popcorn") noise characteristics. Type CA6741, a low-noise version of the CA741, gives limit specifications for burst noise in the data bulletin, File No. 530. Contact your RCA Sales Representative for information pertinent to other operational amplifier types that meet low-burst noise specifications.

"G" Suffix Types—Hermetic Gold-CHIP in Dual-In-Line Plastic Package
"E" Suffix Types—Standard Dual-In-Line Plastic Package
"T" and "S" Suffix Types—TO-5 Style Package

Features:

- Input bias current (all types): 500 nA max.
- Input offset current (all types): 200 nA max.

Applications:

- Comparator
- DC amplifier
- Integrator or differentiator
- Multivibrator
- Narrow-band or band-pass filter
- Summing amplifier

MAXIMUM RATINGS, *Absolute-Maximum Values at T_A = 25°C:*

DC Supply Voltage (between V⁺ and V⁻ terminals):	
CA741C, CA747C*, CA748C, CA1458*	36 V
CA741, CA747*, CA748, CA1558*	44 V
Differential Input Voltage	±30 V
DC Input Voltage**	±15 V
Output Short-Circuit Duration	Indefinite
Device Dissipation	
Up to 70°C (CA741C, CA748C)	500 mW
Up to 75°C (CA741, CA748)	500 mW
Up to 30°C (CA747)	800 mW
Up to 25°C (CA747C)	800 mW
Up to 30°C (CA1558)	680 mW
Up to 25°C (CA1458)	680 mW
For Temperatures Indicated Above	Derate linearly 6.67 mW/°C
Voltage between Offset Null and V⁻ (CA741C, CA741, CA747CE, CA747CG)	±0.5 V
Ambient Temperature Range	
Operating— CA741, CA747E, CA748, CA1558	−55 to +125 °C
CA741C, CA747C, CA748C, CA1458	0 to +70 °C†
Storage	−65 to +150 °C
Lead Temperature (During Soldering):	
At distance 1/16 ± 1/32 inch (1.59 ± 0.79 mm) from case for 10 seconds max.	265 °C

* If Supply Voltage is less than ± 15 volts, the Absolute Maximum Input Voltage is equal to the Supply Voltage

** Voltage values apply for each of the dual operational amplifiers.

† All types in any package style can be operated over the temperature range of −55 to +125°C, although the published limits for certain electrical specifications apply only over the temperature range of 0 to +70°C.

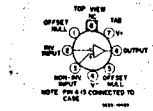

1a.–CA741CS,CA741CT,CA741S, & CA741T with internal phase compensation.

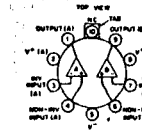

1b.–CA747CT and CA747T with internal phase compensation.

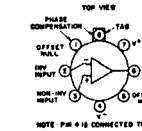

1c.–CA748CS, CA748CT,CA748S, and CA748T with external phase compensation.

Fig. 1 – Functional diagrams.

RCA Type No.	No. of Ampl.	Phase Comp.	Offset Voltage Null	Min. A_{OL}	Max. V_{IO} (mV)	Operating-Temperature Range (°C)
CA1458	dual	int.	no	20k	6	0 to +70*
CA1558	dual	int.	no	50k	5	−55 to +125
CA741C	single	int.	yes	20k	6	0 to +70*
CA741	single	int.	yes	50k	5	−55 to +125
CA747C	dual	int.	yes*	20k	6	0 to +70*
CA747	dual	int.	yes*	50k	5	−55 to +125
CA748C	single	ext.	yes	20k	6	0 to +70*
CA748	single	ext.	yes	50k	5	−55 to +125

*In the 14-lead dual-in-line plastic package only.

*All types in any package style can be operated over the temperature range of −55 to +125°C, although the published limits for certain electrical specifications apply only over the temperature range of 0 to +70°C.

ORDERING INFORMATION

When ordering any of these types, it is important that the appropriate suffix letter for the package required be affixed to the type number. For example: If a CA1458 in a straight-lead TO-5 style package is desired, order CA1458T.

Type No.	PACKAGE TYPE AND SUFFIX LETTER										FIG. No.
	TO-5 STYLE			PLASTIC		Gold-CHIP PLASTIC		CHIP	Gold-CHIP	BEAM-LEAD	
	8L	10L	DIL-CAN	8L	14L	8L	14L				
CA1458	T		S	E		G		H	GH		1d, 1h
CA1558	T		S	E		G					1d, 1h
CA741C	T		S	E		G		H	GH		1a, 1e
CA741	T		S	E		G				L	1a, 1e
CA747C		T			E		G	H	GH		1b, 1f
CA747		T			E		G				1b, 1f
CA748C	T		S	E		G		H	GH		1c, 1g
CA748	T		S	E		G					1c, 1g

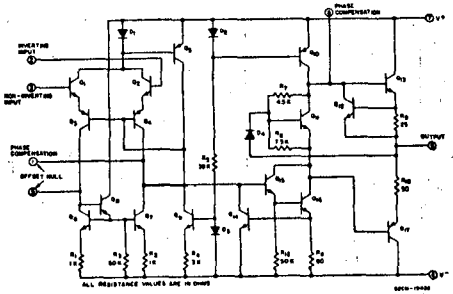

Fig. 2–Schematic diagram of operational amplifier with external phase compensation for CA748C and CA748.

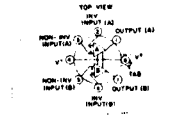

1d.–CA1458S,CA1458T,CA1558S, and CA1558T and internal phase compensation.

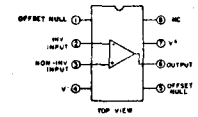

1e.–CA741CE,CA741CG,CA741E, and CA741G with internal phase compensation.

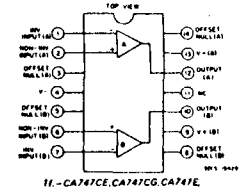

1f.–CA747CE,CA747CG,CA747E, and CA747G with internal phase compensation.

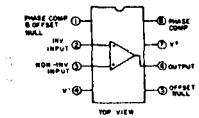

1g–CA748CE,CA748CG,CA748E, and CA748G with external phase compensation.

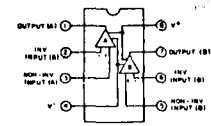

1h.–CA1458E,CA1458G,CA1558E, and CA1558G with internal phase compensation

Fig. 1 – Functional Diagrams (Cont'd)